Supporting Information

A scalable top-down strategy toward practical metrics of Ni-Zn battery with total energy density of 165 Wh/kg and 506 Wh/L

Wanhai Zhou,[a,c] *Ding Zhu,*[*,a] *Jian He,*[a] *Jinchi Li,*[a] *Hui Chen,*[b] *Yungui Chen,*[*,a,b] *Dongliang Chao*[*,c]

[a] Institute of New-Energy and Low-Carbon Technology, Sichuan University, Chengdu, Sichuan, China, 610065.

[b] College of Materials Science and Technology, Sichuan University, Chengdu, Sichuan, China, 610065.

[c] School of Chemical Engineering & Advanced Materials, The University of Adelaide, Adelaide, SA 5005, Australia.

SUPPLEMENTARY METHODS

Preparation of $Ni_{0.95}Zn_{0.05}(OH)_{2.0}$ and NiS-coated $Ni_{0.95}Zn_{0.05}(OH)_{2.0}$ microspheres

All the reagents utilized were of analytical grade and were used directly without any purification. $Ni_{0.95}Zn_{0.05}(OH)_{2.0}$ microspheres can be easily prepared by using a traditional co-precipitation method. Briefly, $NiSO_4·6H_2O$ and $ZnSO_4·6H_2O$ were dissolved in Milli-Q water (>18 MΩ cm) with a molar ratio of Ni: Zn=95: 5 and the concentration of the solution is 2.0 mol L^{-1}. The mixed solution was put into a CSTR (continuous stirred tank reactor) with a capacity of 2 L. Simultaneously, 2.0 mol L^{-1} solution of NaOH and 0.5 mol L^{-1} solution of NH_4OH as a chelating agent were separately pumped into the CSTR. The reaction was conducted at 50 °C for 10 h while maintaining a pH value in a range of 11-11.2. Afterwards, the co-precipitated powders were collected by filtration, washed by Milli-Q water until the pH of the filtered solution was within 7.1-7.6, and finally dried at 80 °C for overnight to obtain the product of $Ni_{0.95}Zn_{0.05}(OH)_{2.0}$ microspheres.

To obtain NiS-coated $Ni_{0.95}Zn_{0.05}(OH)_{2.0}$ microspheres, 2.4 g of as-prepared sample was immersed in the 0.2 M sodium sulfide ($Na_2S·9H_2O$) solution and then transferred into 50 mL Teflon-lined stainless-steel autoclave and heated at 120 °C for 2 h. After being cooled to room temperature gradually, the colour of the powders changed to black from green of uncoated samples, and finally, the product was collected after carefully filtering, washing and drying.

Alkaline Zn-Ni battery design

A home-made Ni-Zn demo battery (Figure S11), is employed to prevent the activated hydrogen evolution reaction of zinc anode by iron or nickel materials in standard 2025 coin cell, which is harmful to battery sealing. The sealed aqueous Ni-Zn alkaline battery was assembled using an activated NiS-coated $Ni_{0.95}Zn_{0.05}(OH)_{2.0}$ as cathode and a Zn-mesh with the same area as anode. And a mixed aqueous solution consisting of 4 M KOH, 2 M KF, 1 M K_2CO_3 and saturated ZnO was used as the electrolyte. The amount of electrolyte is controlled under a lean-liquid level of 100 μL. Typically, the cathodes were fabricated by dispersing 96 wt% active materials, 3 wt% acetylene black (conductive agent), and 1 wt% polytetrafluoroethylene (PTFE, binder) in Milli-Q water to form a homogeneous slurry, followed by casting the slurry into nickel foam (32 mg cm^{-2}, Hunan Corun New Energy Co., Ltd), and dried at 80 °C overnight in a vacuum oven. Then, all electrodes were compressed to a thickness of 500 μm, followed by cutting into disks with a diameter of 14 mm.

The typical mass loading was about 80.0 mg cm^{-2}, unless otherwise stated. The Zn mesh anode was facile fabricated onto brass mesh *via* electrodeposition with an aqueous solution of 6 M KOH with saturated ZnO at a constant current of 50 mA cm^{-2} for 45 min. The areal mass loading of the Zn-mesh was around 42 mg cm^{-2}. The cathode and anode of the sealed cells were separated by a hydride separator (CL-FH-140, Henan Chaoli New Energy Co., Ltd), where the polyolefin microporous membrane used for preventing dendrite and the Nonwoven used for electrolyte absorption. Ni/Cu foil was used as a tab for the electrodes, which was separated and not in direct contact with the electrolyte so as to avoid any side reactions.

Material Characterization

The crystal structure of all samples was identified by X-ray diffraction (XRD) using a CX-2700 diffractometer with Cu K_{α} radiation at 40 kV and 30 mA. Tapping density of the sample was tested using a JZ-7 tap-density tester. Cold field-emission scanning electron microscope (FESEM, Hitachi SU8230) with energy-dispersive X-ray spectroscope (EDS, Oxford-Instruments X-Max Extreme) was employed to observe the morphology and element distribution of the samples. TEM and HRTEM (FEI Tecnai G2 F20) were performed using a Tecnai G2-F20 operated at 200 kV. XPS was performed employing a ThermoFisher EScalab 250Xi XPS system. The electrical conductivities were measured using an ST-2258C multifunction digital four-probe system, which equipped with an SZT-D semiconductor powder resistivity tester.

Electrochemical measurements

Cyclic voltammetry (CV) and EIS tests were performed on MULTI AUTOLAB M204 electrochemical workstation. Before electrochemical measurements, all of the batteries were activated after 3 CV cycles within 1.35-2.1 V at 3 mV s^{-1}. EIS tests were conducted using a sine perturbation signal of 5 mV in the frequency range of 10 KHz - 10 mHz. The obtained spectra were fitted using the software ZSimpWin 3.1. Galvanostatic intermittent titration technique (GITT) was obtained by a series of galvanostatic discharge pulses of 180 s at 0.2C (4.48 mA cm^{-2}) followed by a 30 min rest.

The electrochemical performance of Ni-Zn demo batteries was carried out using a LANDCT2001A battery tester. For the rate performance, the batteries were firstly fully charged at 1C (280 mA $g^{-1}_{cathode}$ *i.e.* 22.4 mA cm^{-2}), and then discharged to a cutoff potential of 1.4 V at

different current densities from 1C to 20C (5600 mA $g^{-1}_{cathode}$ *i.e.* 448 mA cm^{-2}). The specific capacities of batteries were calculated from the discharge curves, according to the equation of $C = (I \times \Delta t)/A$, where C is specific discharge capacity, I is the discharge current, Δt is the discharge time, and A is the mass of active materials or the area of the electrodes. Here, to reliably evaluate the electrochemical performance of the batteries, energy and power densities were calculated based on the total mass of active materials in cathode and anode, except for special illustration. The cycling tests were conducted at 2C within 1.4-2.0 V, and 10C within 1.2-2.1 V. To measure the peak power density, the batteries were fully charged at 1C, and subsequently discharged at various current densities for 30 s after 30 min of standing. To simulate the frequency modulation in the power grid and validate their applicability for start-stop batteries, long-term high-rate pulse cycling tests were conducted at 10C for 30 s within 60~80% of state of charge (SOC).

Soft-packed batteries preparation

To evaluate the practical application of NiS-coated $Ni_{0.95}Zn_{0.05}(OH)_{2.0}$ cathode materials, serials commercial-grade 3.5 Ah Ni-Zn soft-packed batteries were fabricated. Typically, the mass loading of the cathodes is controlled at around 160 mg cm^{-2}, and then the electrodes were compressed to a thickness of 560 μm, followed by cutting into rectangles with a size of 50 × 180 mm. The anode was fabricated by dispersing Zn powder (76%), ZnO powder (20%), acetylene black (2 wt%), Bi_2O_3 (1 wt%) and PTFE (1 wt%) in Milli-Q water to form a homogeneous slurry, followed by casting the slurry into brass mesh current collector, and dried at 80 °C overnight in a vacuum oven. The typical mass loading of which was about 70.0 mg cm^{-2}, all electrodes were compressed to a thickness of 150 μm, followed by cutting into rectangles with a size of 50 × 180 mm. The negative to positive active material capacity ratio (N/P) is controlled within 1.2-2, and the detailed parameters of the Ni-Zn soft-packed batteries are listed in Table S4. The cathodes, anodes and separators (55 × 380 mm) were then stacked layer by layer and rolled with an MSK-112A winding machine (the width of the winding mould is 40 mm). The NiS-coated $Ni_{0.95}Zn_{0.05}(OH)_{2.0}$ cathodes were fully activated before usage. Then, the above-rolled components were transferred into an aluminum-plastic pouch, followed by injecting an appropriate amount of 4M KOH + 2M KF + 1M K_2CO_3 + saturated ZnO electrolyte. Finally, coupled with tab-film, the Ni-Zn pouch batteries were sealed using an MSK-140L machine. All of the above operations were conducted in ambient air without any extra protection.

Electrochemical measurements

The electrochemical performances of Ah-level Ni-Zn full batteries were performed using a Neware battery testing system (CT-4002-10V100A). For the rate performance, the batteries were firstly fully charged at 0.7 A (0.2C), and then discharged to a cutoff potential of 1.2 V at different current densities from 0.7 A to 42 A (12C). The cycling tests were conducted at 3.5 A within the voltage range of 1.2-2.0 V.

Calculation of proton diffusion coefficient

In CV method, the proton diffusion coefficient D_H can be calculated based on the Sevick equation:

$$i = 2.69\times10^5 \times n^{3/2} \times A \times D_H^{1/2} \times C_0 \times v^{1/2} \quad \text{(S1)}$$

where n is the electron transfer number ($n\approx1$ for $Ni(OH)_2$), A is the surface area of the electrode (A=1.5386 cm^2), and C_0 is the proton concentration (0.04408 mol cm^{-3} for $Ni(OH)_2$ derived from the theoretical density of 4.1 g cm^{-3}).

In GITT tests, the discharge current pulse was set at 56 mA g^{-1} for 3 min and the battery relaxed for 30 min to reach voltage equilibrium. This procedure is repeated during the entire discharge process. The diffusion coefficient is calculated from:

$$D_{GITT} = \frac{4}{\pi\tau}\left(\frac{mV}{MS}\right)^2\left(\frac{\Delta E_s}{\Delta E_\tau}\right)^2 \quad \text{(S2)}$$

where τ refers to the duration of the current pulse, E_τ is the potential for this duration, m, V and M are, respectively, the mass, molar volume (cm^3 mol^{-1}) and molecular weight (g mol^{-1}) of the active material. S is the contact area of the electrode in the electrolyte, and; ΔE_s is the difference in open circuit voltage, measured at the end of the relaxation period of two successive steps. The equation is simplified in the condition of a linear relationship of $dE_\tau/d\tau^{1/2}$ and $\tau < L^2/D_{GITT}$ where L is electrode thickness.

Cost estimation for electrode materials and full Ni-Zn battery device

It is conservatively estimated that the price for $Ni(OH)_2$ (63.3% of Ni content) is 7.105 US$ kg^{-1} (http://www.infomine.com/investment/nickel/ accessed March 31, 2020) and that for zinc is 1.848 US$ kg^{-1} (http://www.infomine.com/investment/zinc/ accessed March 31, 2020). The price of separator (US$0.42 m^{-2}) and KOH (US$1 kg^{-1}) are obtained from Alibaba.com. Thus, the estimated combined cost for the negative and positive active material would be calculated as:

$$(m_A \times P_A + m_C \times P_C)/E_d = (0.08 \times 7.105 + 0.042 \times 1.848)/(0.08*266.6*1.71/1000) = 17.71 \text{US\$ kWh}^{-1} \quad \text{(S3)}$$

where P_A and P_C correspond to, respectively, the price of anode and cathode in US$ kg^{-1}; and E_d is the delivery energy in kWh. As a result, based on the total mass of active materials in cathode and anode, an ultrahigh energy density of 298.9 Wh kg^{-1} can be achieved, and the materials cost of the Ni-Zn battery is as low as USD $17.7 per kWh. The cost of the aqueous 6 M KOH electrolyte is almost negligible when comparing this technology to batteries operating with a non-aqueous electrolyte. Additional costs would slightly arise from cell components and housing, and detailed cost calculation of the 3.5 Ah commercial-grade pouch Ni-Zn battery cell is exhibited in Table S6. As a result, its cost is only USD $32.8 per kWh. Additionally, the manufacturing cost for positive electrode and batteries is anticipated to be low, owing to the aqueous processing method and the facile fabrication of batteries in ambient air negating complicated procedures or extra protection.

Cost estimation of Co species in cathode

Cobalt is an important strategic resource with limited reserves and geographical distribution. The increasing or volatile price of Co has become increasingly acute.[1] The price of Co is 29. 5 US$ kg^{-1} (http://www.infomine.com/investment/metal-prices/cobalt/all/ accessed March 31, 2020), but it once reached as high as 119 and 94.2 US$ kg^{-1}, respectively, in March 2008 and March 2018. As a result, the Co species in cathode inevitably increase the cost. If there is 6 *w.t* % Co content in $Ni(OH)_2$ and extra 5 *w.t* % CoO are need in the electrodes preparation process,[2] the cost of cathode material will be up to 9.2-17.3 US$ kg^{-1}, which is around 30-143% higher than our Co-free cathode.

Table S1. Electrochemical performance of various advanced cathode materials for alkaline Zn battery and supercapacitors reported in recent years.

Cathode types	Mass loading /mg cm^{-2}	Specific capacity mAh g^{-1}	Rate performance / %	Cycle performance / %	Ref.
NiS-coated $Ni_{0.95}Zn_{0.05}(OH)_{2.0}$	**80**	**266.6 at 22.4 mA cm^{-2}**	**84.2 at 448 mA cm^{-2}**	**81.4 800 cycles at 44.8 mA cm^{-2}** **79.2 3500 cycles at 224 mA cm^{-2}**	**This work**
Commercial Co-coated Co,Zn-doped $Ni(OH)_2$	80	238.8 at 22.4 mA cm^{-2}	39.9 at 448 mA cm^{-2}	42.3 800 cycles at 44.8 mA cm^{-2}	
Alkaline Zn batteries					
NiAlCo LDH/CNT	1	354 at 6.7 A g^{-1}	78.5 at 66.7 A g^{-1}	94 2000 cycles at 66.7 A g^{-1}	3
	46	300 at 0.145 mA g^{-1}	–	–	
NNA@CNH	0.49	346 at 5 A g^{-1}	45.7 at 30 A g^{-1}	90 5000 cycles at 30 A g^{-1}	4
	3.89	275 at 5 A g^{-1}	–	–	
Ni_3S_2@PANI	3.86	247.6 at 11.4 A g^{-1}	66.7 at 22.8 A g^{-1}	125 10000 cycles at 17.1 A g^{-1}	5
NiCo-90	1.56	303.6 at 1.28 A g^{-1}	80 at 25.6 A g^{-1}	–	6
SANF	–	0.422 mAh cm^{-2} at 8 mA cm^{-2}	52.4 at 40 mA cm^{-2}	75.4 5000 cycles at 8 mA cm^{-2}	7
CC-CCH@CMO	2.78	260.2 at 360 mA g^{-1}	67.6 at 23.02 A g^{-1}	71.1 5000 cycles at 29 A g^{-1}	8
P-$NiCo_2O_{4-x}$	0.66	309.2 at 6 A g^{-1}	64 at 60.4 A g^{-1}	81.8 3000 cycles	9
$NiCo_2O_4$	1.2	230.1 at 0.5 A g^{-1}	71.4 at 8 A g^{-1}	63.2 1000 cycles at 1 A g^{-1}	10
$NiCo_2O_4$@CC	0.313	183.1 at 1.6 A g^{-1}	52.5 at 32 A g^{-1}	82.7 3500 at 6.4 A g^{-1}	11
Ni_2P/C	1	176 at 1 A g^{-1}	46.6 at 5 A g^{-1}	93.8 1500 cycles at 5 A g^{-1}	12
NiO	–	3200 μAh cm^{-3} at 8 mA cm^{-2}	30.6 at 20 mA cm^{-2}	84.8 10000 cycles at 10 mA cm^{-2}	13
Ni-NiO-3	–	237.8 μAh cm^{-3} at 3.7 A g^{-1}	74.4 at 37 A g^{-1}	98.9 10000 at 18.5 A g^{-1}	14
Co_3O_4@NF	2	162 at 1 A g^{-1}	48.1 at 10 A g^{-1}	80 2000 cycles at 1 A g^{-1}	15
CC-CF@NiO	1.32	265 at 3.78 A g^{-1}	63.2 at 45.45 A g^{-1}	92.4 6000 cycles	16
NiO/CNTs	3	155 at 1 A g^{-1}	52.9 at 3 A g^{-1}	65 500 cycles at 1 A g^{-1}	17
Co_3O_4@NiO	12	242.4 at 0.314 A g^{-1}	60.5 at 3.14 A g^{-1}	96 1000 cycles at 3.14 A g^{-1}	18
Ni_3S_2@NF	–	148 at 0.2 A g^{-1}	45.9 at 5 A g^{-1}	100 100 cycles	19
β-$Ni(OH)_2$/CNFs	2	208 at 5 A g^{-1}	84.1 at 50 A g^{-1}	100 1000 cycles at 10 A g^{-1}	20
α-$Ni(OH)_2$/C	1	331 at 1 A g^{-1}	76.4 at 12 A g^{-1}	85 500 cycles at 12 A g^{-1}	21
Ni_2P	0.5	242 at 1 A g^{-1}	76.1 at 20 A g^{-1}	86 5000 cycles at 6 A g^{-1}	22
α/β-$Ni(OH)_2$/CNF	10	215 at 1.5 A g^{-1}	85.1 at 5 A g^{-1}	91 1200 cycles at 100 mV s^{-1}	23
Supercapacitors					
$NiSe_2$/$Ni(OH)_2$	2.5	253 at 1 A g^{-1}	65.7 at 20 A g^{-1}	85 5000 cycles at 5 A g^{-1}	24
β-$Ni(OH)_2$/GO/CNTs	1	277 at 2 A g^{-1}	47.2 at 20 A g^{-1}	97 2000 cycles at 10 A g^{-1}	25
NiCo-LDH@CNT	8.5	284 at 1 A g^{-1}	65.4 at 15 A g^{-1}	78 1200 cycles at 1 A g^{-1}	26
NiMn-LDH/PC	3.2	191 at 1 A g^{-1}	60.4 at 10 A g^{-1}	85 3000 cycles at 15 A g^{-1}	27
Ni–Co–P/POx	3	180 at 1 A g^{-1}	67 at 50 A g^{-1}	94 1000 cycles	28
NiAl-LDH	1	219 at 1 A g^{-1}	56 at 20 A g^{-1}	93.8 10000 cycles at 20 A g^{-1}	29
Ov-NiMn-LDH	0.345	328 at 1 A g^{-1}	63.8 at 30 A g^{-1}	95 5000 cycles at 20 A g^{-1}	30
$NiCo_2S_4$	5	158 at 1 A g^{-1}	68.1 at 20 A g^{-1}	87 2000 cycles at 5 A g^{-1}	31
$NiCo_2S_4$/Ni_3S_2	10.33	250 at 0.5 A g^{-1}	25 at 20 A g^{-1}	91.4 8000 cycles at 2 A g^{-1}	32

[a] Electrochemical performance of the cathodes obtained from literature was measured in an opening three-electrode system. The capacity of the supercapacitors cathode is transformed by the equation: capacity= capacitance × Δ*E*/3.6.

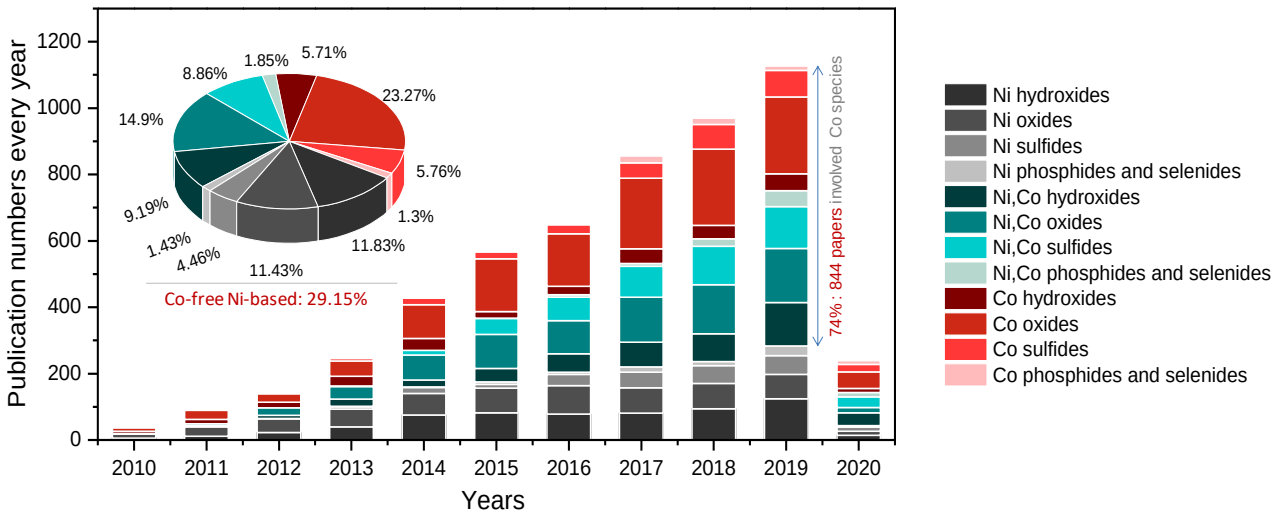

Figure S1. Graphical overview of papers published on the aqueous Ni,Co-based electrochemistry within the last decade, showing an increasing tendency of using Co-based species. (The data were collected from *Web of Science* covered the publications before February 2020.) Note that although some Co-free Ni-based materials have been studied, the Co-free policy or concept has never been clearly proposed in aqueous electrochemistry (include supercapacitors and batteries). And the electrochemical performance of those materials are generally conducted at a low mass-loading level or with large amounts of conductive additives (e.g. 10~20% carbon black), which will make the negative of Co absence unapparent; but under an industrial level with high mass loadings and little conductive additives, to date, there is still no successful case that can completely eliminate Co in the cathode. Note that, nearly all of Ni-based batteries (Ni-MH, Ni-Cd, Ni-Fe and Ni-Zn) are still completely dependent on traditional cobalt-contained $Ni(OH)_2$ cathode.

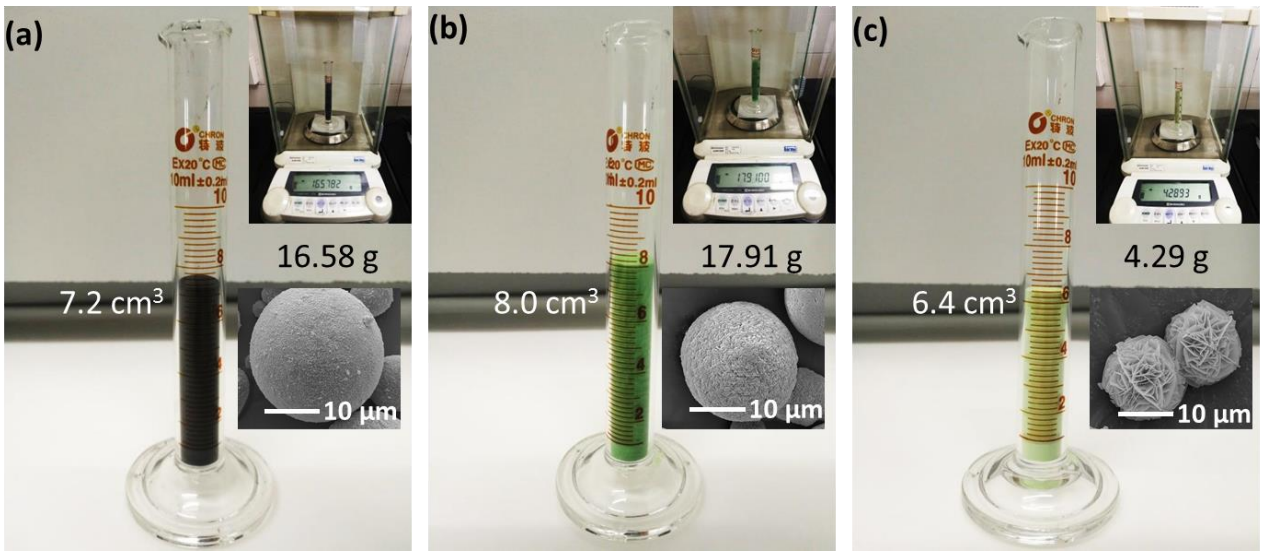

Figure S2. Digital photograph showing the measurement of tap density. The results show a high tap density of ~2.30 g cm^{-3} for black NiS-coated $Ni_{0.95}Zn_{0.05}(OH)_2$ microsphere (a), ~2.24 g cm^{-3} for green $Ni_{0.95}Zn_{0.05}(OH)_2$ microsphere (b), and a low tap density of 0.67 g cm^{-3} for flower-like hierarchical $Ni(OH)_2$ microspheres (c) synthesized according to *ref.* [33].

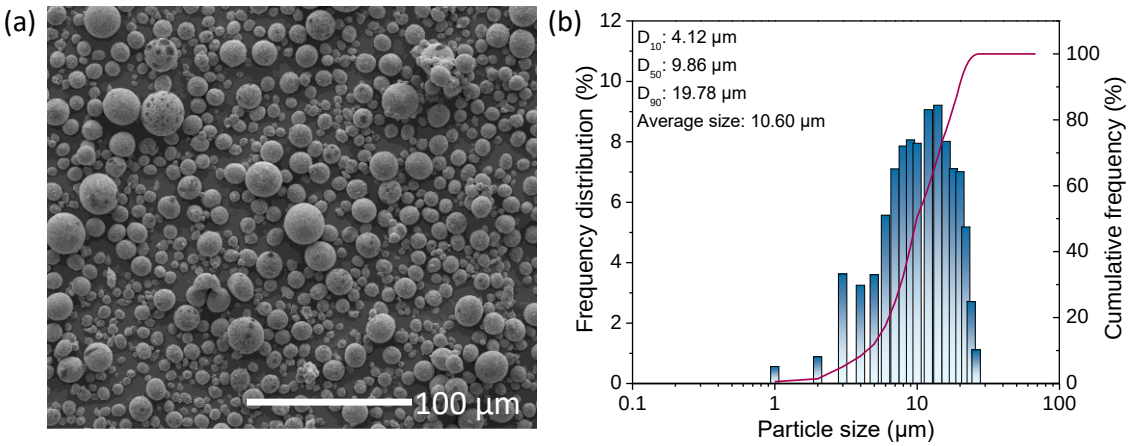

Figure S3. The size distribution of NiS-coated $Ni_{0.95}Zn_{0.05}(OH)_2$ microsphere. a) Low-magnification SEM image. b) Particle size obtained from JL-1155 laser particle size analyzer.

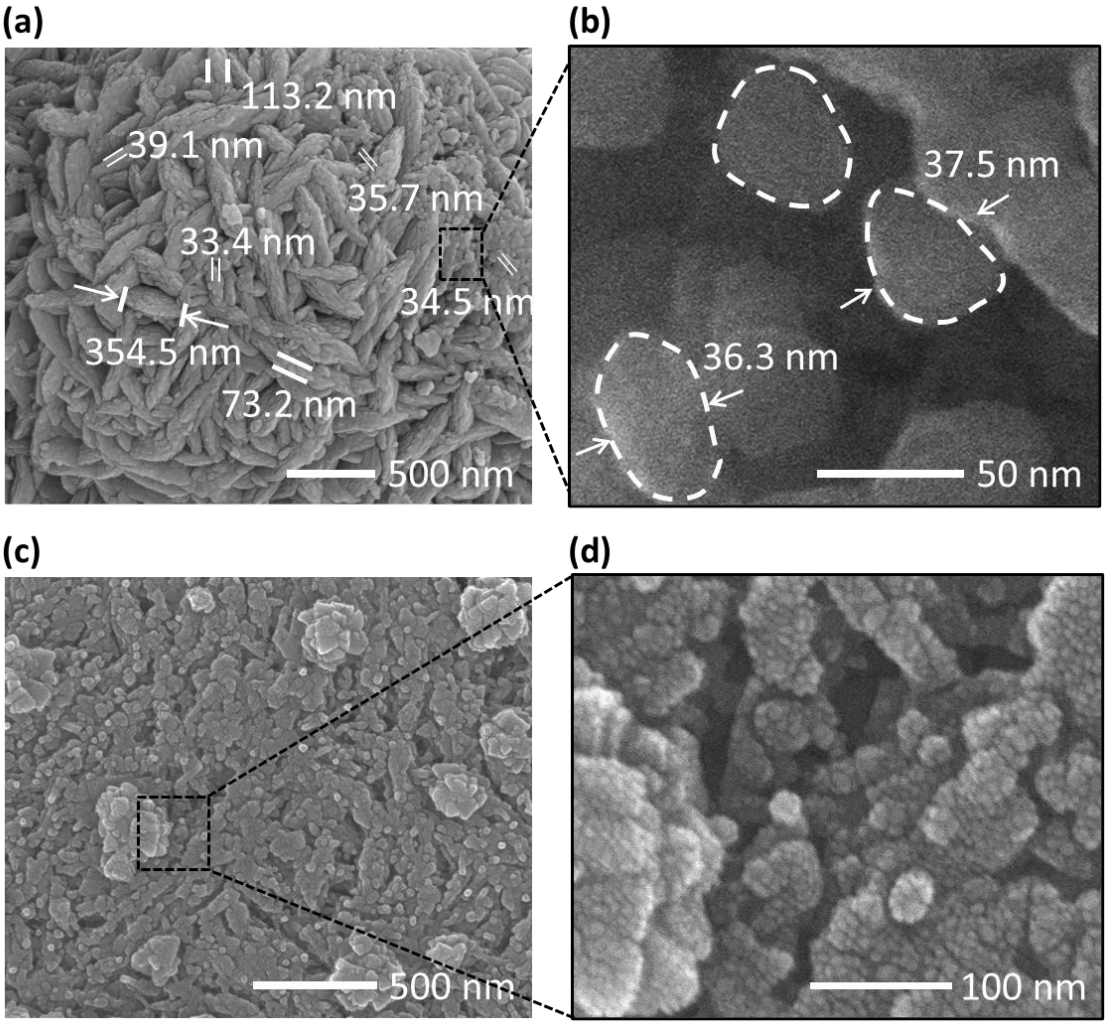

Figure S4. High-magnification SEM images of $Ni_{0.95}Zn_{0.05}(OH)_2$ precursor and NiS-coated $Ni_{0.95}Zn_{0.05}(OH)_2$ microsphere. a,b) $Ni_{0.95}Zn_{0.05}(OH)_2$ precursor is composed of spindle nanostructure with 50-120 nm in width and 300-400 nm in length. The spindle nanostructure consists of ultrafine nanoparticles with an average size of ~38 nm. c,d) NiS-coated $Ni_{0.95}Zn_{0.05}(OH)_2$ microsphere. The results show that the surface nanoparticles with a size of ~300 nm are assembled by equiaxial nanoparticles with an average size of ~7.0 nm.

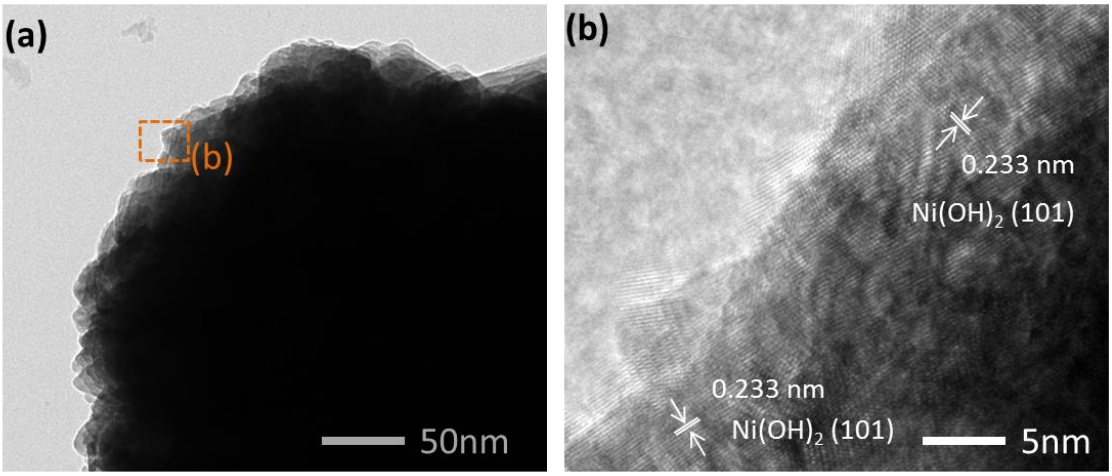

Figure S5. TEM (a) and HRTEM (b) images of $Ni_{0.95}Zn_{0.05}(OH)_2$ microsphere. $Ni_{0.95}Zn_{0.05}(OH)_2$ microsphere is also constituted by a compact core and a relatively porous surface, the corresponding HRTEM reveals that the crystalline interplanar spacing taken from the outer layer (orange region), is measured to be approximately 0.233 nm, well matching that of the (101) lattice planes of β-$Ni(OH)_2$ phase.

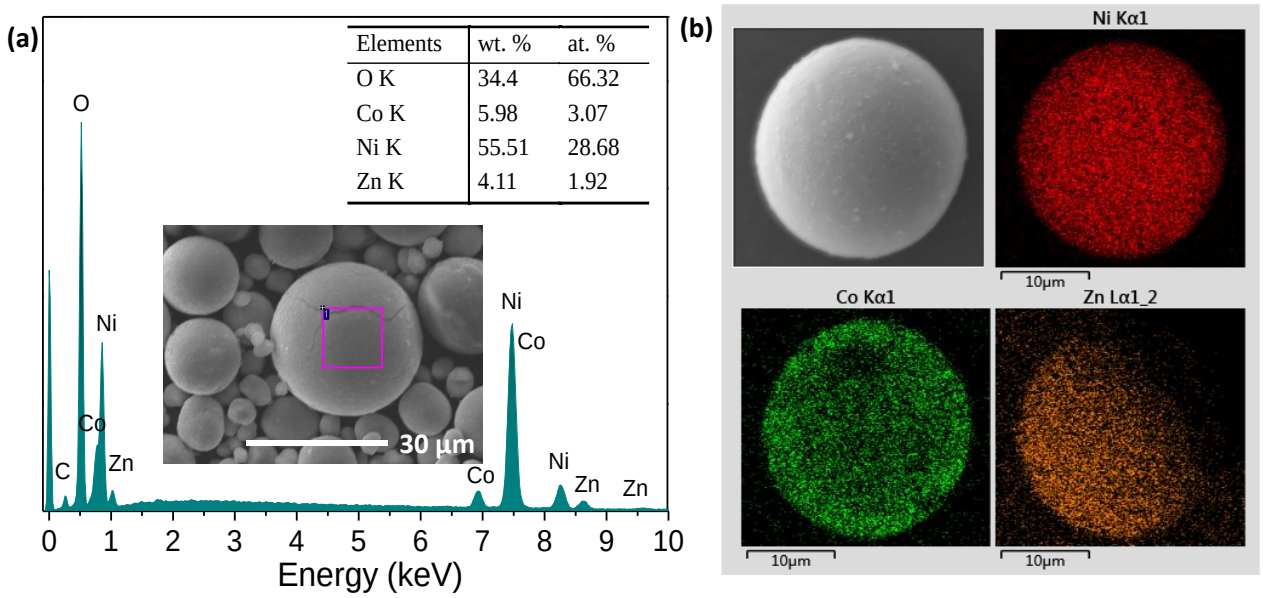

Figure S6. Composition analysis of the commercial Co-coated Co,Zn-doped Ni(OH)$_2$ microsphere. a) EDS spectrum showing that the Co content in commercial cathode is as high as 5.98 wt.%, which increases around 12% of cost. b) EDS mapping of the elements distribution of Ni, Co, Zn in commercial cathode.

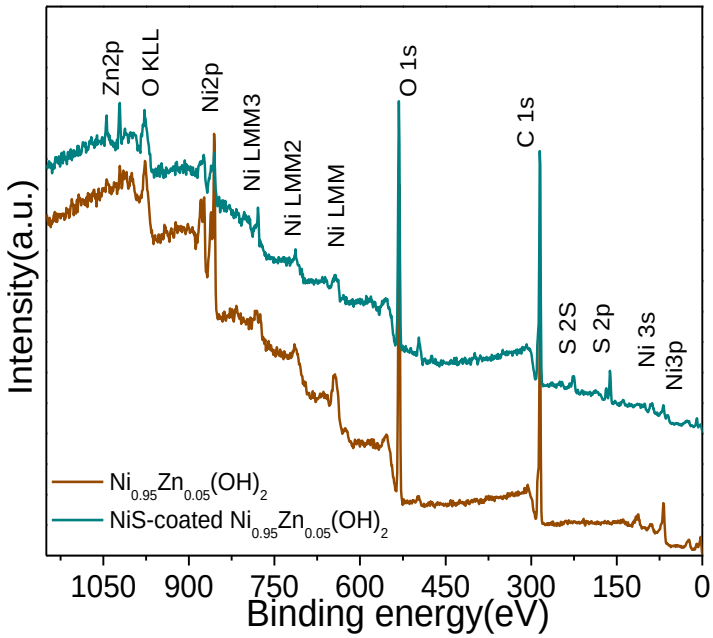

Figure S7. Composition characterization of $Ni_{0.95}Zn_{0.05}(OH)_2$ and NiS-coated $Ni_{0.95}Zn_{0.05}(OH)_2$ microsphere. Survey XPS spectra of $Ni_{0.95}Zn_{0.05}(OH)_2$ and NiS-coated $Ni_{0.95}Zn_{0.05}(OH)_2$ microsphere.

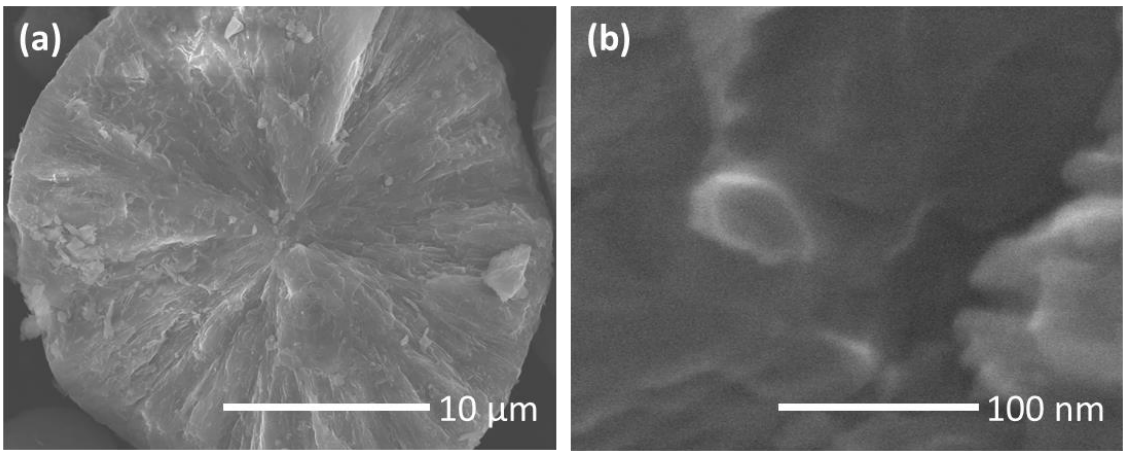

Figure S8. SEM images of the interior of the $Ni_{0.95}Zn_{0.05}(OH)_2$ microsphere. a) Low-magnification SEM image showing the dense structure in the bulk of $Ni_{0.95}Zn_{0.05}(OH)_2$ microsphere. b) High-magnification SEM image.

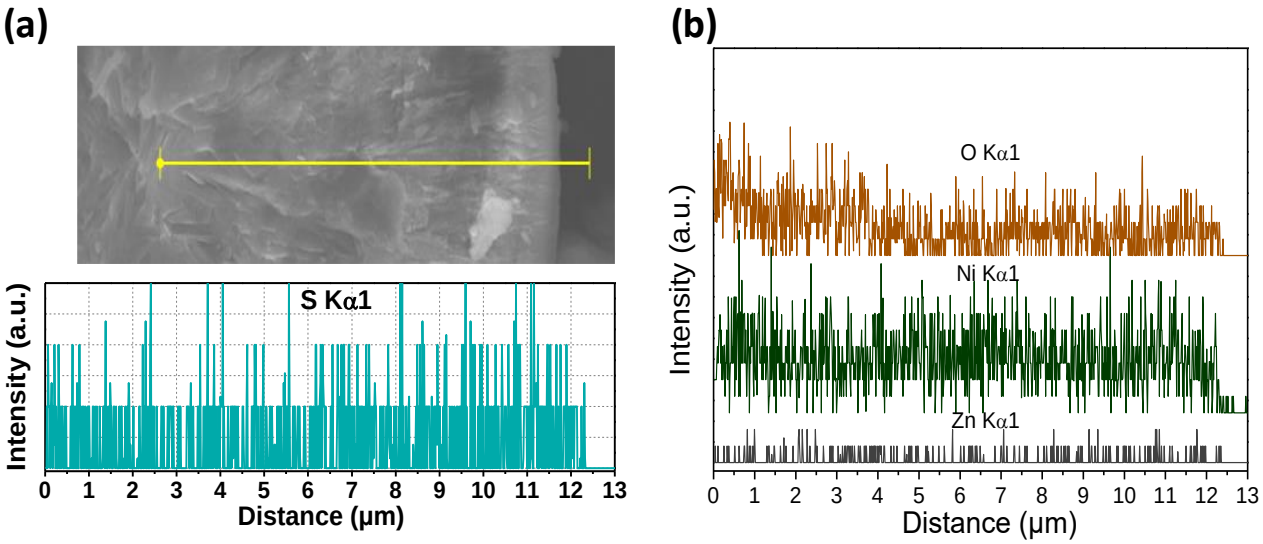

Figure S9. EDS line scanning results of S O, Ni and Zn elements distribution in the interior of the NiS-coated $Ni_{0.95}Zn_{0.05}(OH)_2$ microsphere.

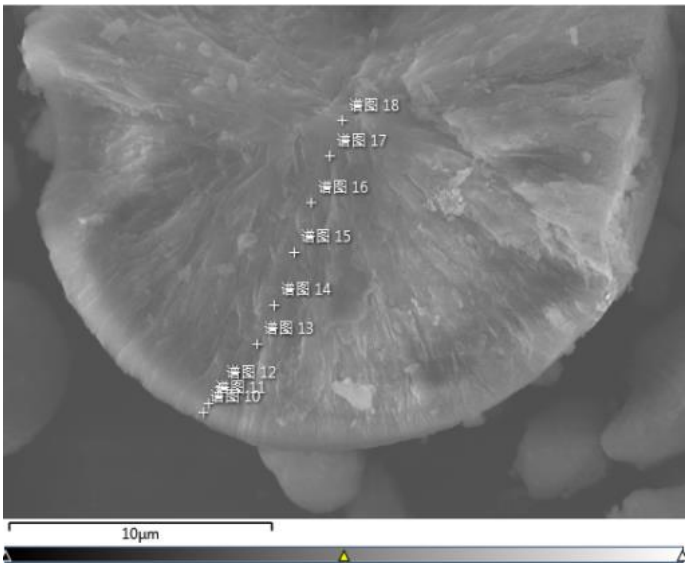

Figure S10. SEM image showing the location of EDS dot scan for composition analysis in the interior of the NiS-coated $Ni_{0.95}Zn_{0.05}(OH)_2$ microsphere.

Table S2. EDS results in elements content from the area identified in SEM micrograph (Figure S9).

Location	Elements content wt. %			
	Ni	Zn	O	S
10	65.8	3.6	26.8	3.8
11	63.7	3.9	28.7	3.7
12	63.2	3.8	29.8	3.2
13	62.7	3.9	30.5	2.9
14	62.4	3.8	30.9	2.9
15	61.7	4	31.6	2.7
16	61.8	3.8	31.7	2.7
17	61.4	3.7	32.4	2.5
18	56.7	3.3	37.5	2.5

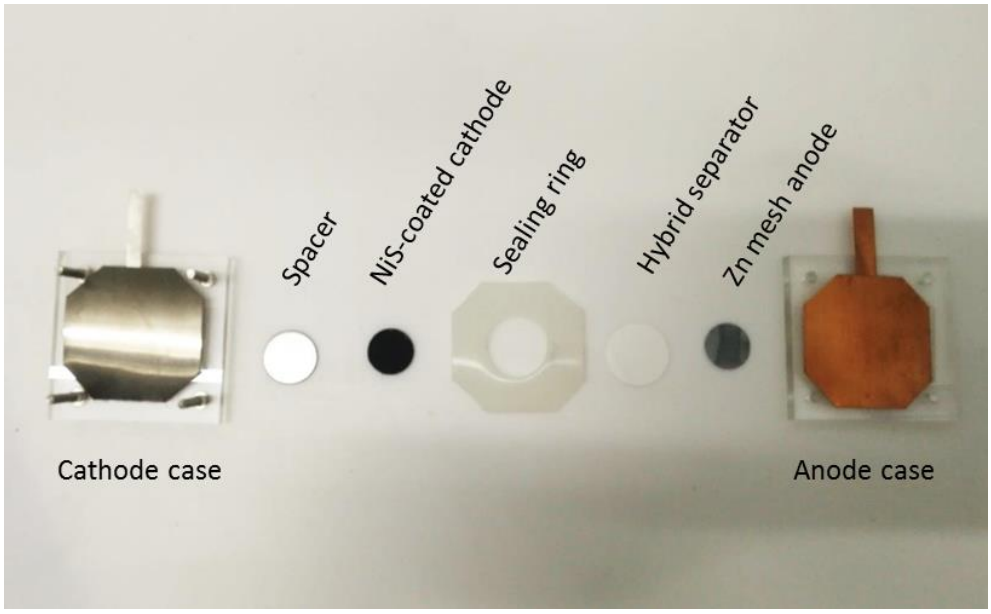

Figure S11. Digital photograph of the home-made Ni-Zn cell. Assembly drawing of the Ni-Zn cell with NiS-coated $Ni_{0.95}Zn_{0.05}(OH)_2$ cathode and Zn mesh anode with the diameter of ϕ 14 mm. The N/P ratio was controlled at 1.6.

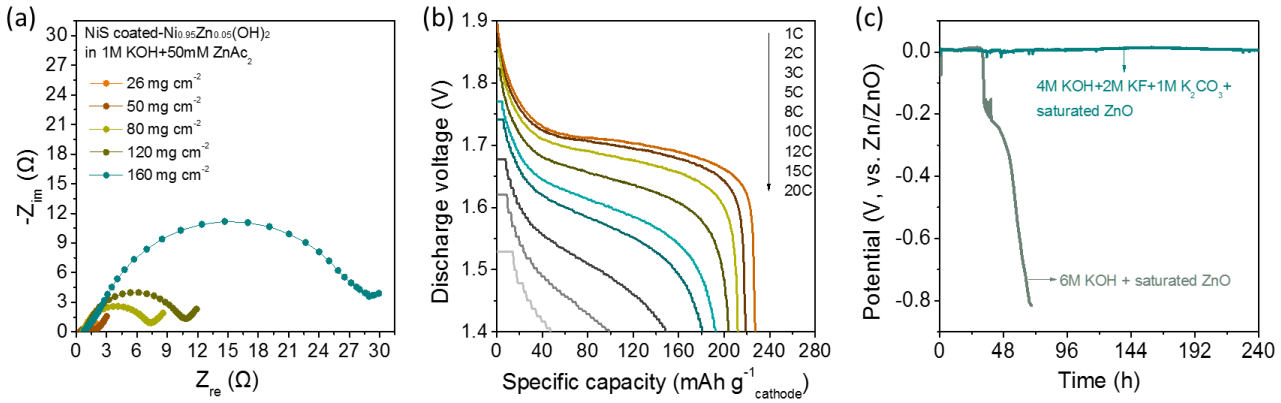

Figure S12. Electrochemical performance in different electrolytes. a) Nyquist plots of the NiS-coated $Ni_{0.95}Zn_{0.05}(OH)_2$ electrode in 1 M KOH + 50 mM $ZnAc_2$ with different mass loadings. b) Galvanostatic discharge profiles of the NiS-coated $Ni_{0.95}Zn_{0.05}(OH)_2$ electrode in 1 M KOH + 50 mM $ZnAc_2$. c) OCV curves of Zn mesh anodes (10 mAh cm^{-2}) in a starved symmetric battery with different electrolytes, showing the less stability in the electrolyte of 6 M KOH + saturated ZnO.

About the electrolyte

As summarized in Table S1, the electrochemical performances were commonly evaluated in a liquid-rich condition, and the cathode materials are usually porous at a low mass-loading-level. As a result, the 1 M KOH electrolyte is applicable in those studies. However, KOH electrolyte with low-concentration is not viable for high mass loading conditions especially in a starved electrolyte environment (Figure S12a,b), considering the slow charge-transfer process, severe concentration polarization and serious ohmic polarization. On the other hand, the high supersaturation of a high concentration electrolyte (e.g. 6M KOH) will cause severe corrosion of Zn anode (Figure S12c) and dissolution of ZnO,[2, 34] resulting in fast battery failure.

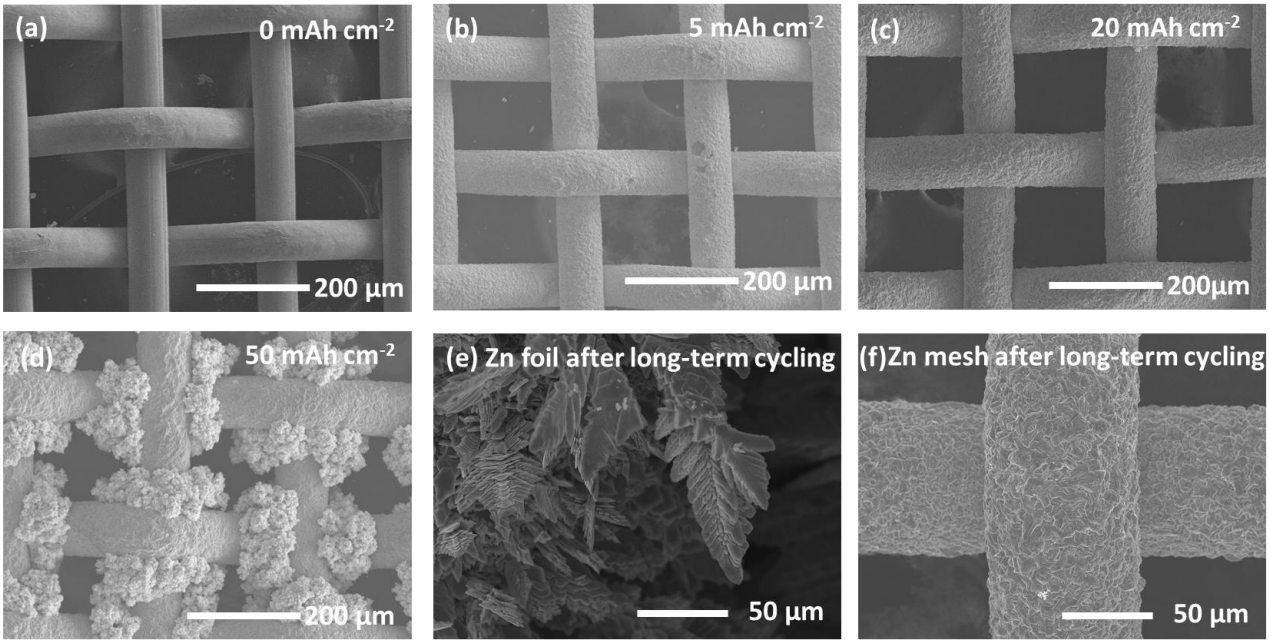

Figure S13. SEM images of Zn mesh based on brass mesh. a) Bare brass mesh. b-d) Zn mesh with areal capacity of 5, 20 and 50 mAh cm^{-2}, respectively. e) Zn foil and f) Zn mesh anodes after 300 cycles.

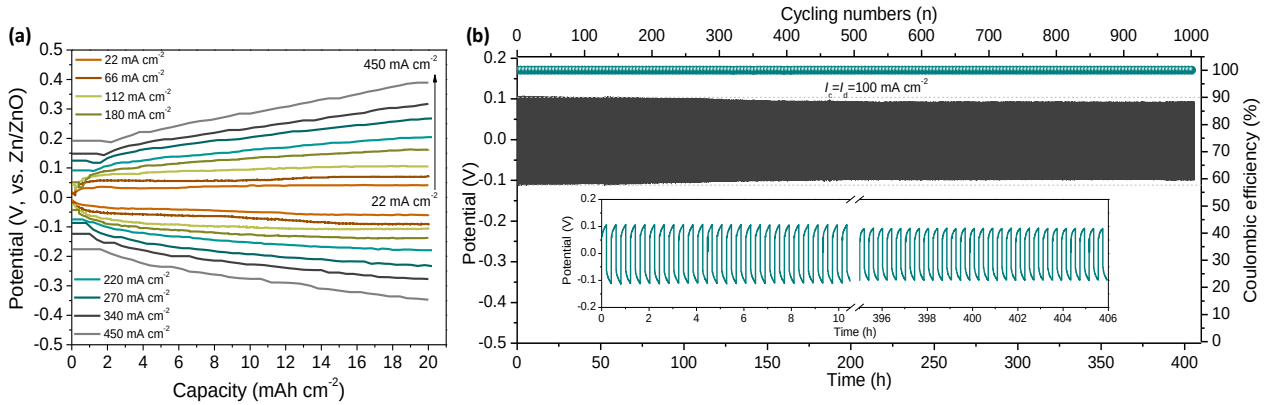

Figure S14. Electrochemical performance of Zn mesh anode. a) Charge/discharge curves. b) Cycling performance at a current density of 100 mA cm^{-2}.

About the Zn anode

The brass mesh used here acts as a current collector for electron transfer and a substrate for electrodeposition of metal Zn. As shown in Figure S13, the interconnected skeleton structure and micron-scale holes (~25537 μm^2) of the brass mesh lead to a uniform distribution of metal Zn mesh anode and a high areal specific capacity (~50 mAh cm^{-2}). Furthermore, this metal Zn mesh anode presents excellent high-rate dischargeability (HRD) and coulombic efficiency (CE). As shown in Figure S14, the symmetric battery used the Zn mesh (31 mAh cm^{-2}) as an anode and Zn foil (200 μm) as a cathode can be charged/discharged at a current of 450 mA cm^{-2} within 0.5 V of potential polarization. When this symmetric battery suffers a long period charge/discharge cycling at a discharge current of 100 mA cm^{-2}, the coulombic efficiency is nearly 100% and the capacity of the Zn mesh anode still can be maintained at 20 mAh cm^{-2} after 1000 cycles. This result confirms the availability of Zn mesh anode with interconnected skeleton and porous structure for high-power and long-life Ni-Zn battery in the electrolyte of 4 M KOH + 2 M KF + 1 M K_2CO_3 with saturated ZnO.

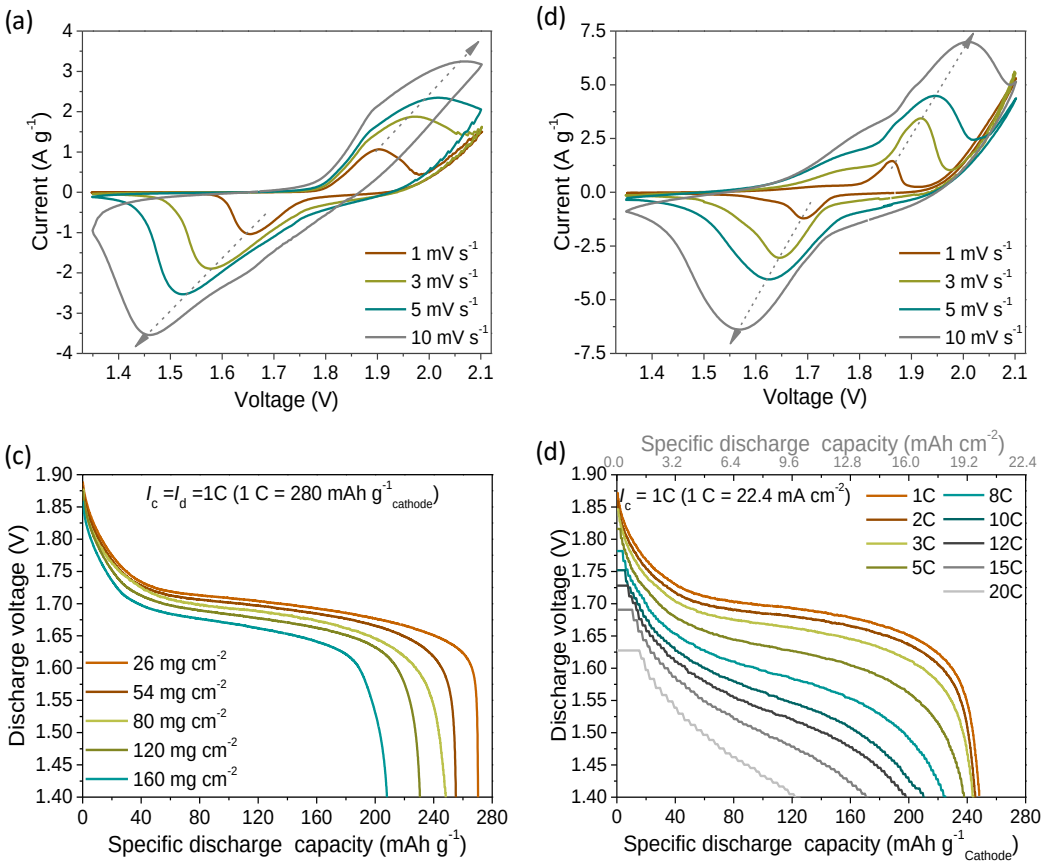

Figure S15. Typical CVs and galvanostatic discharge profiles of the Ni-Zn. a,b) CV curves of $Ni_{0.95}Zn_{0.05}(OH)_2$ (a) and NiS-coated $Ni_{0.95}Zn_{0.05}(OH)_2$ (b) cathodes at various scan rates. c) Galvanostatic discharge profiles of $Ni_{0.95}Zn_{0.05}(OH)_2$ electrode with different mass loadings of cathode materials at current densities of 1 C. d) Galvanostatic discharge profiles of the $Ni_{0.95}Zn_{0.05}(OH)_2$ electrode at various current densities.

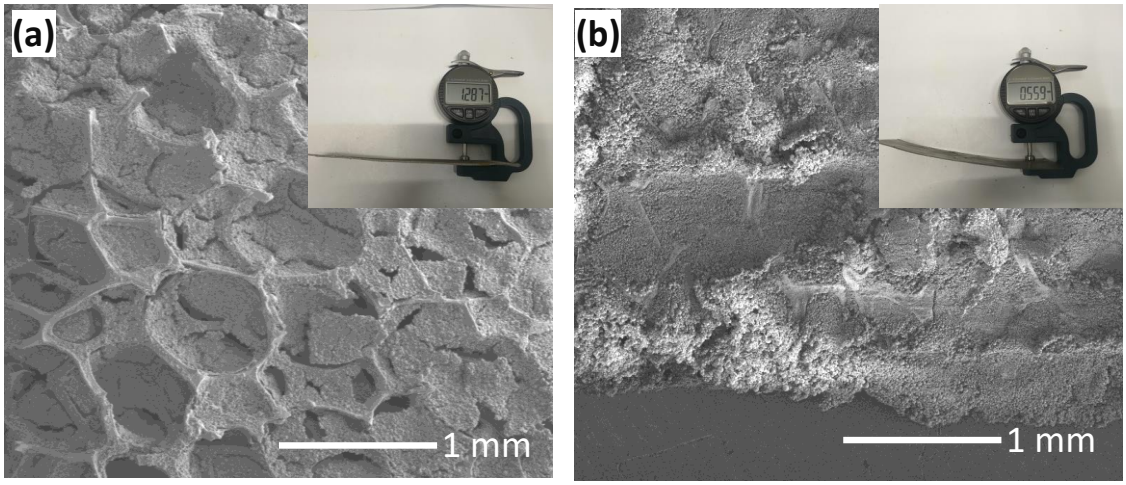

Figure S16. SEM images and thickness of the NiS-coated $Ni_{0.95}Zn_{0.05}(OH)_2$ cathode with high mass loading of 160 mg cm^{-2}. (a) Before compressing. (b) After compressing to 560 μm of thickness. The insets show the thickness of 1287 μm for the loose cathode, and the thickness of 559 μm for the compacted cathode.

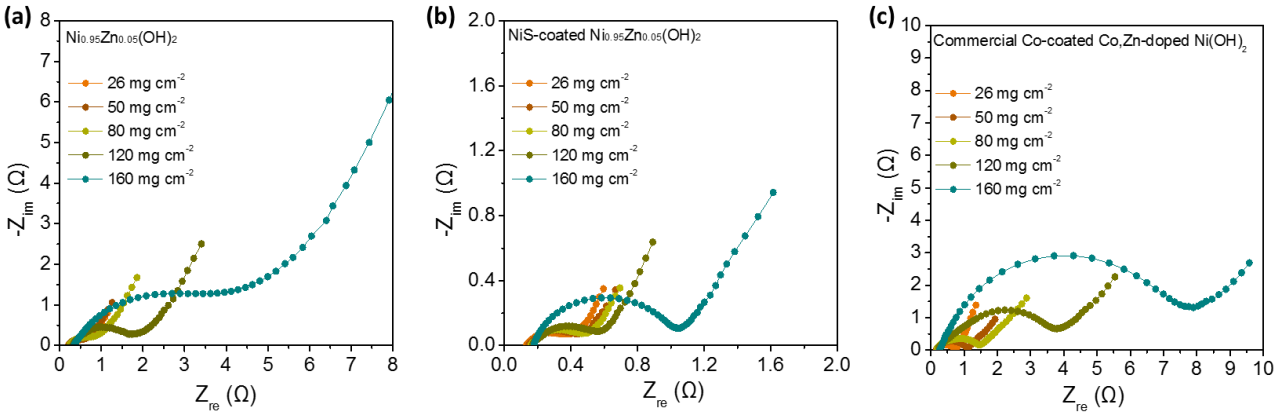

Figure S17. Nyquist plots of the electrodes with different mass loadings. a) $Ni_{0.95}Zn_{0.05}(OH)_2$. b) NiS-coated $Ni_{0.95}Zn_{0.05}(OH)_2$. c) Commercial Co-coated Co,Zn-doped $Ni(OH)_2$.

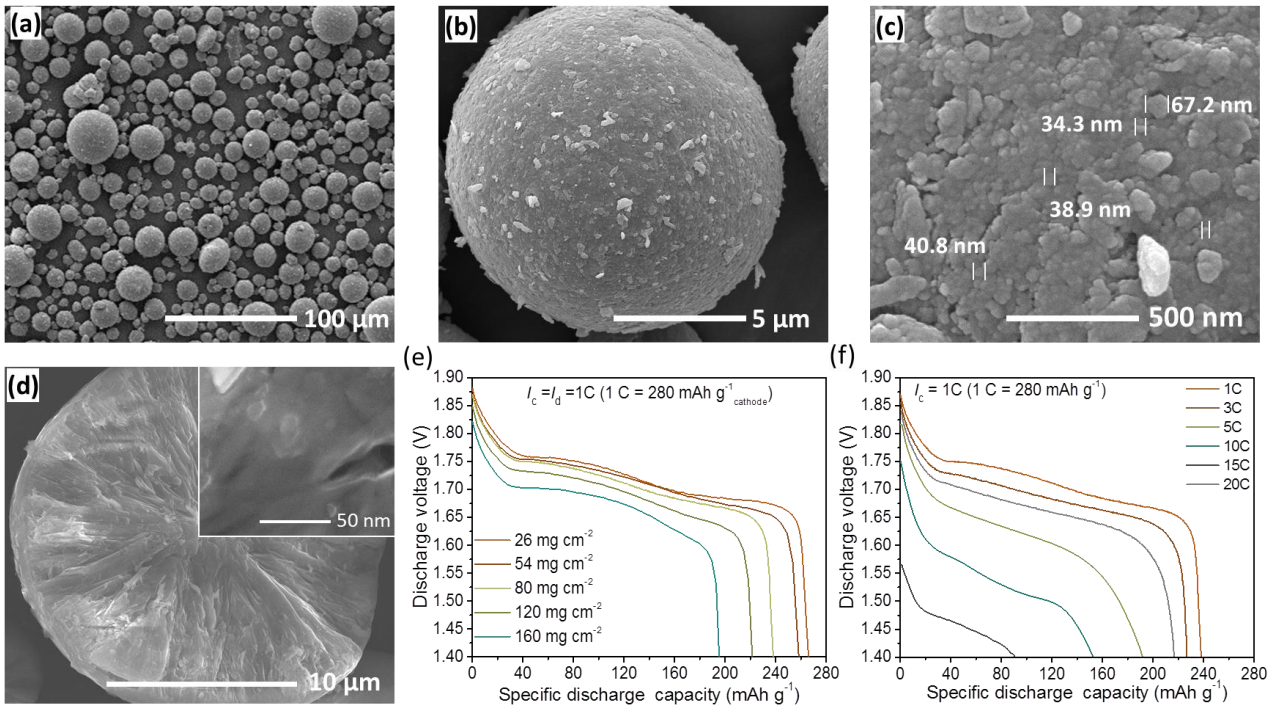

Figure S18. Material characterization and electrochemical performance of the commercial Co-coated Co,Zn-doped Ni(OH)$_2$ microsphere. a-d) SEM images. e) Typical galvanostatic discharge profiles of the Co-coated Co,Zn-doped Ni(OH)$_2$//Zn batteries with different cathode loadings at 1 C. f) Galvanostatic discharge curves of the commercial Co-coated Ni(OH)$_2$ microsphere with mass loading of 80 mg cm^{-2} at different current densities from 1 C to 20 C.

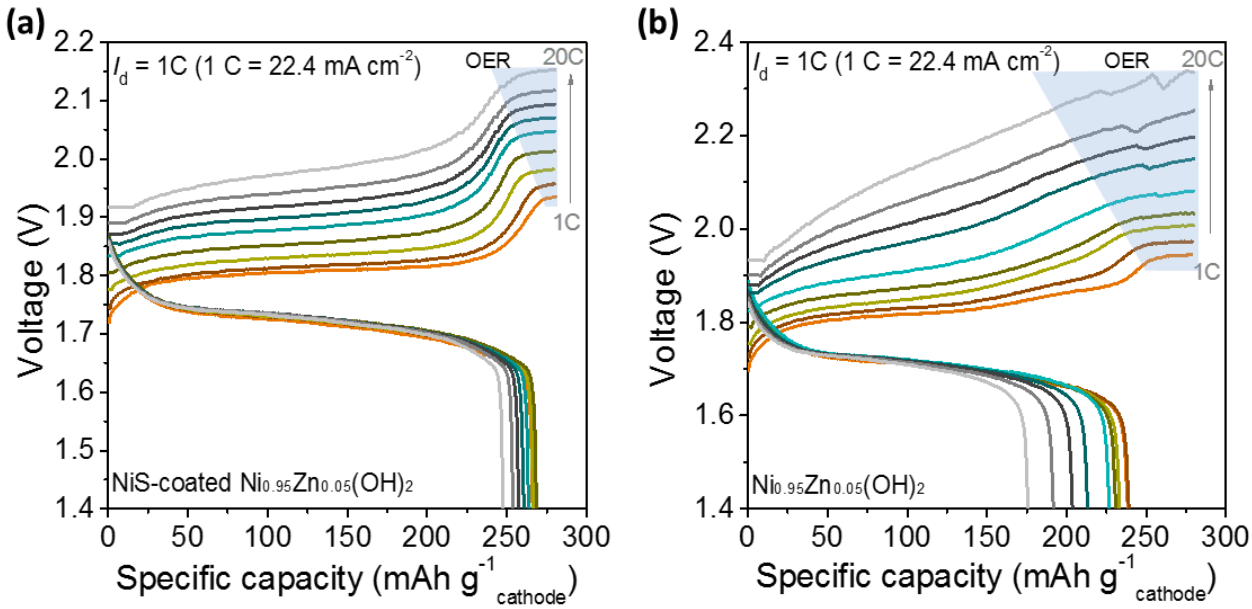

Figure S19. High-rate chargeability of the electrodes. a) NiS-coated $Ni_{0.95}Zn_{0.05}(OH)_2$. b) $Ni_{0.95}Zn_{0.05}(OH)_2$.

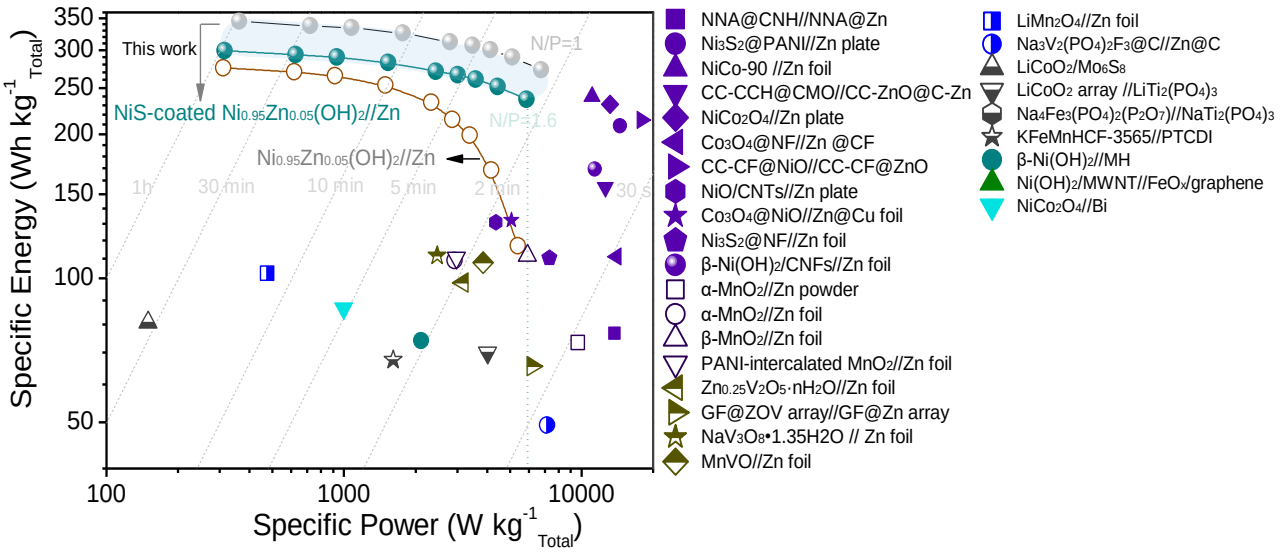

Figure S20. Ragone plots showing the gravimetric energy density and power density based on the total mass loading of cathode and anode active materials.

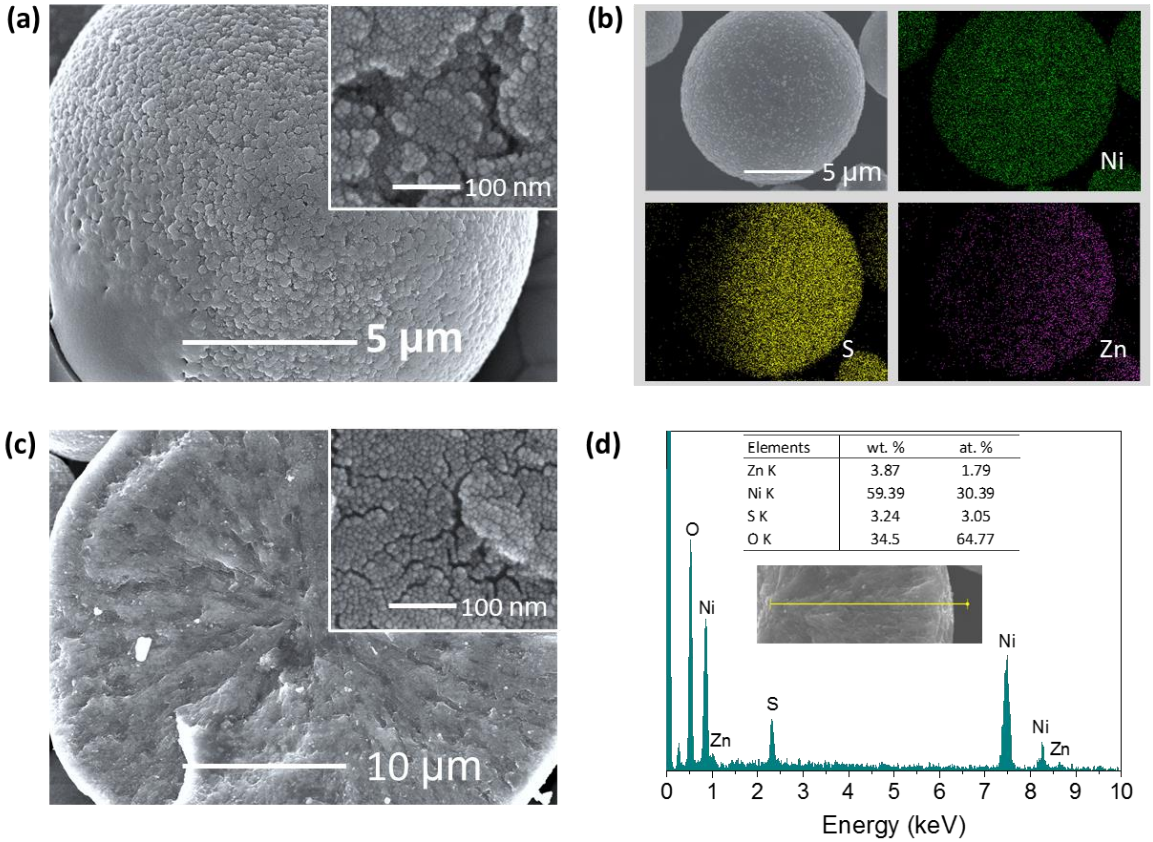

Figure S21. Microstructure and composition analysis of NiS-coated $Ni_{0.95}Zn_{0.05}(OH)_2$ cathode materials after 50 cycles. a) SEM image of the microsphere. Inset shows the well maintaining of the equiaxial nanoparticles with an average size of ~7.0 nm in the surface. b) EDS mapping shows a homogeneous distribution of Ni, Zn and S elements after cycles. c) Cross-section SEM image of the inner structure. d) EDS spectrum indicates that the S element is well maintained after cycles.

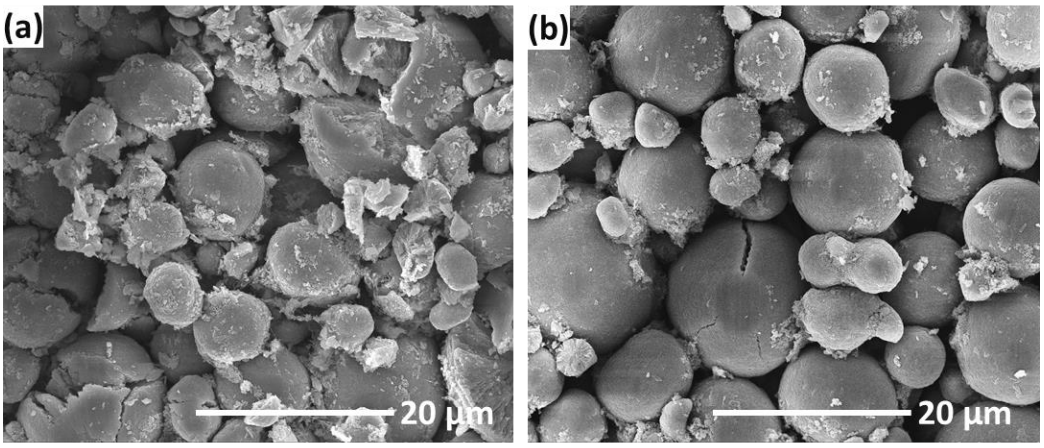

Figure S22. SEM images of the cathode after 800 cycles. (a) $Ni_{0.95}Zn_{0.05}(OH)_2$ cathode. (b) NiS-coated $Ni_{0.95}Zn_{0.05}(OH)_2$ cathode. After long-term cycling, the NiS-coated $Ni_{0.95}Zn_{0.05}(OH)_2$ maintains its initial micro-spherical morphology without microcracks on the surface, further verifying the superior cycling stability after NiS coating.

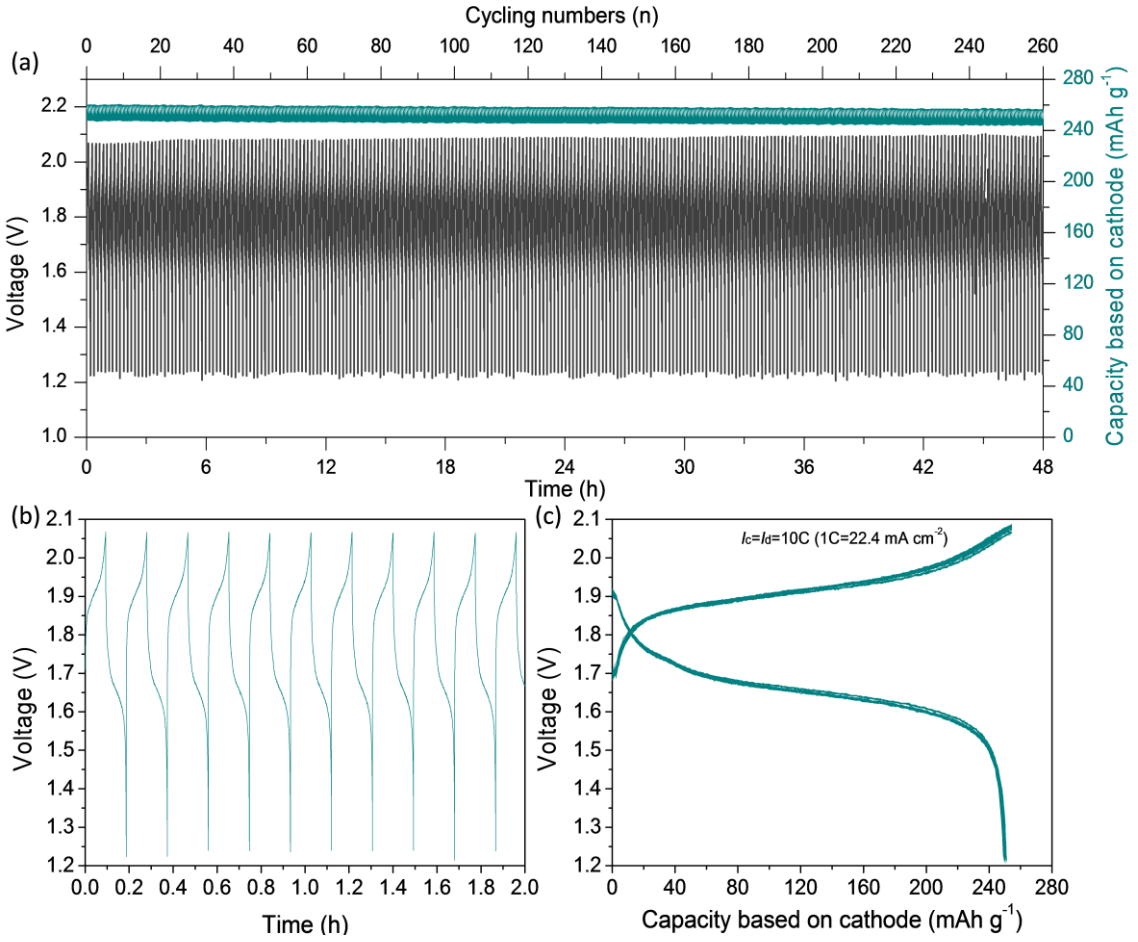

Figure S23. Cycling performance of NiS-coated $Ni_{0.95}Zn_{0.05}(OH)_2$//Zn battery at the current density of 10C. a) Potential evolution as cycles at 224 mA cm^{-2} within a potential window of 1.2-2.1 V, showing the high stability of the battery. b) Galvanostatic curves showing the fast charge/discharge process. c) Charge/discharge curves of the former 100 cycles showing the high capacity utilization with a high coulombic efficiency up to 98.6%.

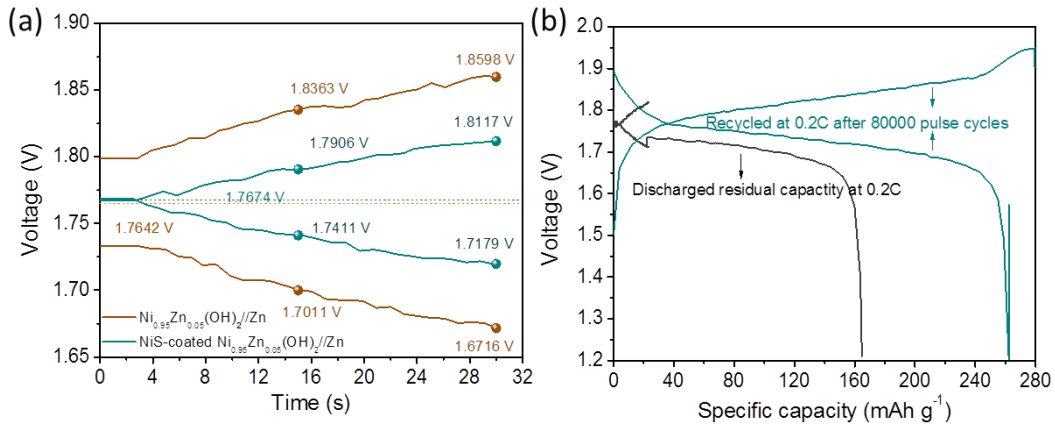

Figure S24. (a) Typical charge-discharge curves of the Ni-Zn batteries pulsed at 10C within 60~80% SOC. (b) The residual discharge and recovery charge/discharge curves of the NiS-coated $Ni_{0.95}Zn_{0.05}(OH)_2$//Zn battery after 80000 pulse cycles. The results show much lower initial voltage polarization in NiS-coated $Ni_{0.95}Zn_{0.05}(OH)_2$ cathode, thereby offering a high energy efficiency of 97.2% (the result of middle discharge voltage divide by middle charge voltage).

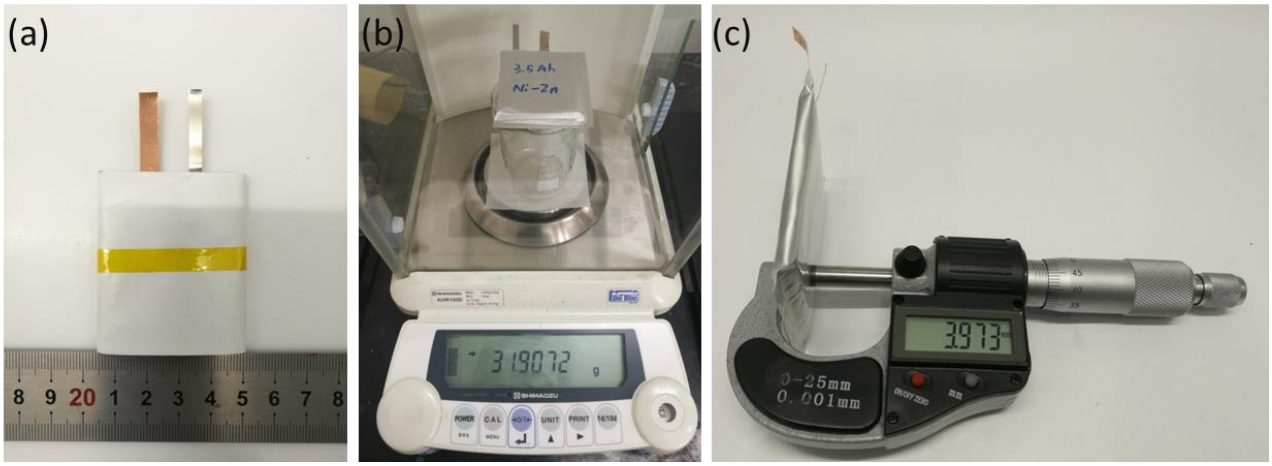

Figure S25. Digital photographs of the 3.5 Ah Ni-Zn soft-package batteries. (a) The rolled components before transferring into an aluminum-plastic pouch. (b) The weight of a typical 3.5 Ah Ni-Zn battery with N/P=1.6. (c) The thickness of a typical 3.5 Ah Ni-Zn battery.

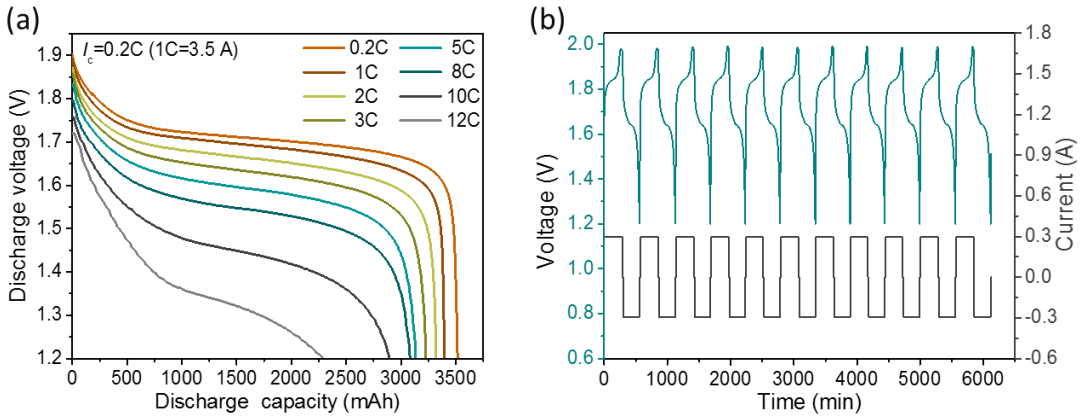

Figure S26. (a) Galvanostatic discharge profiles of NiS-coated $Ni_{0.95}Zn_{0.05}(OH)_2$//Zn pouch cell at different current from 0.7 A to 42 A. (b) Electrochemical performance of commercial AA Ni-Zn battery (BPI). Voltage responds curves at the current density of 0.3 A (0.2C). The results show a fast capacity decay and large voltage polarization in commercial AA Ni-Zn battery.

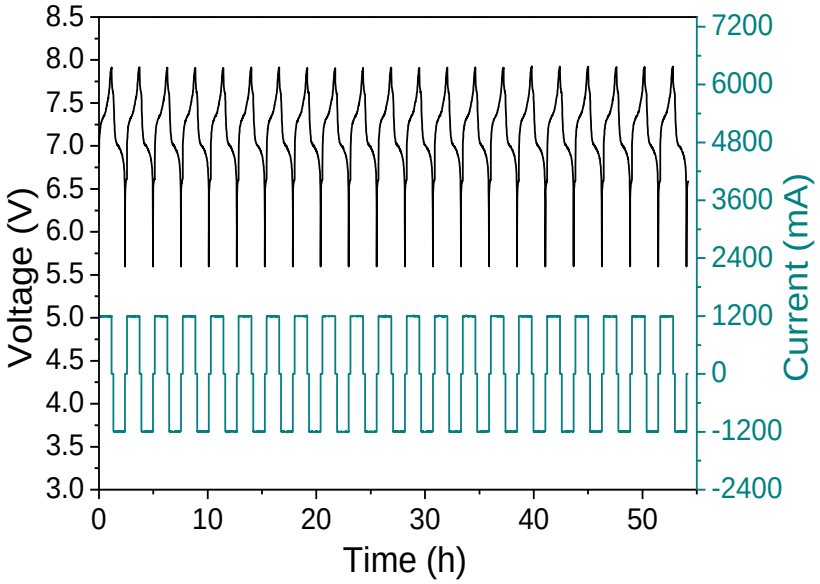

Figure S27. Electrochemical performance of the 7 V, 1.2 Ah Ni-Zn battery fabricated by simply connecting four single cells in series. Voltage responds curves, showing the stable cycling performance of the battery.

Table S3. Rate dischargeability of the Ni-Zn batteries made of $Ni_{0.95}Zn_{0.05}(OH)_2$ and NiS-coated $Ni_{0.95}Zn_{0.05}(OH)_2$ cathodes.

Samples		1C			3C			5C			10C			15C			20C		
		Cap. /mAh g^{-1}	$E_{mid,d}$ /V	W /Wh kg^{-1}	Cap. /mAh g^{-1}	$E_{mid,d}$ /V	W /Wh kg^{-1}	Cap. /mAh g^{-1}	$E_{mid,d}$ /V	W /Wh kg^{-1}	Cap. /mAh g^{-1}	$E_{mid,d}$ /V	W /Wh kg^{-1}	Cap. /mAh g^{-1}	$E_{mid,d}$ /V	W /Wh kg^{-1}	Cap. /mAh g^{-1}	$E_{mid,d}$ /V	W /Wh kg^{-1}
NiS-coated $Ni_{0.95}Zn_{0.05}(OH)_2$	A	266.6	1.7135	456.8	261.4	1.6923	442.4	257.3	1.6757	431.2	247.2	1.6437	406.3	237.7	1.6149	383.9	226.1	1.5973	361.1
	B	174.8		299.6	171.4		290.1	168.7		282.7	162.1		266.4	155.9		251.7	148.3		236.8
$Ni_{0.95}Zn_{0.05}(OH)_2$	A	248.2	1.6918	419.9	243.4	1.6618	404.5	237.6	1.6271	386.6	210.2	1.5573	327.3	169.9	1.5111	256.7	120.9	1.4722	178.1
	B	162.75		275.3	159.6		265.2	155.8		253.5	137.9		214.7	111.4		168.4	79.3		116.8

Two methods were conducted to calculate the capacity of the batteries. The A method is based on the mass of cathode materials, which is important for comparing with various reported cathode materials. The B method is based on the total mass of cathode and anode materials, which is more reliable to reflect the real electrochemical performance of the batteries at materials level.

Table S4. Comparison of the electrochemical performance in different types of aqueous batteries.

Cathode//anode materials	Electrolyte	Voltage /V	Max. gravimetric energy density /Wh kg^{-1} [a]	Gravimetric Energy density at max. power density /Wh kg^{-1} (W kg^{-1})	Max. areal energy density /mWh cm^{-2}	Areal energy density at max. power density /mWh cm^{-2} (mW cm^{-2})	Cycling stability [b] /%	Ref.
NiS-coated $Ni_{0.95}Zn_{0.05}(OH)_2$ // Zn mesh	4M KOH+2M KF+1 M K_2CO_3 + sat. ZnO	1.71	299.6	236.8 (5865.5)	36.5	28.9 (715.6)	81.4 800 cycles at util. 100% 79.1 3500 cycles at util. 94% 100 80000 cycles at util. 10%	This work
$Ni_{0.95}Zn_{0.05}(OH)_2$ // Zn mesh		1.69	275.3	116.8 (5406.1)	33.6	14.2 (659.5)	56.3 800 cycles at util. 100%	
Ni-Zn batteries								
NiAlCo LDH/CNT // Zn@Cu foil	1 M KOH+50 mM $ZnAc_2$	1.75	324.0	225.0 (40000)	0.54	0.37 (66.8)	85.0 600 cycles at util. 84%	3
NNA@CNH // NNA@Zn	1 M KOH	1.75	148.5	76 (13800)	0.25	0.13 (23.0)	88.0 5000 cycles at util. 53%	4
Ni_3S_2@PANI// Zn plate	6 M KOH+0.2 M $ZnAc_2$	1.71	319.7	204.1 (14542)	1.49	0.66 (149.8)	100 5000 cycles at util. 93%	5
NiCo-90 //Zn foil	2.5M KOH + sat. ZnO	1.66	391.7	234.7 (11063)	0.85	0.51 (24.2)	73.0 850 cycles at util. 82%	6
SANF // Zn foil	1 M KOH+20 mM $ZnAc_2$	1.73	–	–	0.75	0.08 (67.6)	92.5 1800 cycles at util. 100%	7
CC-CCH@CMO//CC-ZnO@C-Zn	6 M KOH+1.5 M ZnO	1.65	235.6	152.4 (12610)	1.17	0.75 (62.8)	82.5 1500 cycles at util. 67%	8
P-$NiCo_2O_{4-x}$ // Zn foil	1 M KOH + 50 mM $ZnAc_2$	1.71	427.1	254.2 (20916)	0.41	0.24 (19.9)	71.4 5000 cycles at util. 37%	9
$NiCo_2O_4$ // Zn plate	6 M KOH+0.1 M $ZnAc_2$	1.70	301.5	226.0 (13200)	0.47	0.34 (15.8)	63.2 1000 cycles at util. 97%	10
$NiCo_2O_4$@CC// Zn @CC	1 M KOH + 20 mM $ZnAc_2$	1.71	303.8	159.4 (49000)	0.095	0.049 (15.3)	82.7 3500 cycles at util. 37%	11
NF@NiO // Zn plate	1 M KOH	1.72	–	–	0.0256	0.007 (86.5)	87.0 10000 cycles at util. 30%	13
Ni-NiO // Zn plate	1 M KOH + sat. ZnO	1.75	–	–	0.0066	0.003 (20.2)	99.6 10000 cycles at util. 83%	14
Co_3O_4@NF // Zn @CF	1 M KOH + 10 mM $ZnAc_2$	1.78	241.0	109.5 (14039)	0.57	0.26 (33.6)	80.0 2000 cycles at util. 100%	15
CC-CF@NiO // CC-CF@ZnO	2 M KOH + sat. ZnO	1.75	355.7	210.0 (17900)	0.68	0.40 (34.4)	72.9 2400 cycles at util. 64%	16
NiO/CNTs // Zn plate	1 M KOH + 10 mM $ZnAc_2$	1.75	228.3	129.0 (4368)	0.81	0.43 (15.6)	65.0 500 cycles at util. 100%	17
Co_3O_4@NiO // Zn@Cu foil	6 M KOH	1.72	316.1	130.3 (5074)	5.12	2.11 (82.2)	89.0 500 cycles at util. 43%	18
Ni_3S_2@NF // Zn foil	1 M KOH + 20 mM $ZnAc_2$	1.78	223.3	108.7 (7333)	–	–	100 100 cycles at util. 100%	19
β-$Ni(OH)_2$/CNFs // Zn foil	6 M KOH +1 M LiOH + PAAS + sat. ZnO	1.80	325.0	166 (11400)	3.25	1.66 (114)	96 1200 cycles at util. 46%	20

Neutral Zn-MnO_2 batteries								
α-MnO_2 // Zn powder	1 M $ZnSO_4$	1.3	217.6	72.7 (9653)	–	–	76.9 100 cycles at util. 62%	35
α-MnO_2 // Zn foil	2 M $ZnSO_4$ +0.1 M $MnSO_4$	1.44	288.0	107.5 (2929)	0.39	0.14 (3.9)	92.0 5000 cycles at util. 56%	36
β-MnO_2 // Zn foil	3 M $Zn(OTf)_2$+0.1 M $Mn(OTf)_2$	1.35	254.0	110.0 (5910)	0.70	0.30 (16.2)	94.0 2000 cycles at util. 59%	37
PANI-intercalated MnO_2 // Zn foil	2 M $ZnSO_4$ +0.1 M $MnSO_4$	1.36	295.5	109.1 (2974)	0.80	0.30 (8.1)	89.3 2000 cycles at util. 40%	38
$ZnMn_2O_4$ // TiS_2	2 M $Zn(OTf)_2$	0.87	33.0	–	0.31	–	74.0 100 cycles at util. 100%	39
Neutral Zn-V batteries								
$Zn_{0.25}V_2O_5 \cdot nH_2O$ // Zn foil	1 M $ZnSO_4$	0.71	185.5	96.8 (3173)	1.74	0.91 (29.8)	80.0 1000 cycles at util. 87%	40
GF@ZOV array // GF@Zn array	2M $ZnSO_4$	0.69	140.0	65.0 (6200)	0.784	0.364 (34.7)	89.0 2000 cycles at util. 69%	41
$NaV_3O_8 \bullet 1.35H_2O$ // Zn foil	1 M $ZnSO_4$ +1 M Na_2SO_4	0.73	206.2	110.0 (2474)	0.600	0.220 (5.8)	82.0 1000 cycles at util. 44%	42
MnVO// Zn foil	3 M $Zn(OTf)_2$	0.71	177.6	106.4 (3851)	1.068	0.640 (23.2)	96.0 2000 cycles at util. 65%	43
Zn-based hybrid batteries								
$LiMn_2O_4$ // Zn foil	3M LiCl +4M $ZnCl_2$	1.80	202.1	–	0.594	–	90.0 1000 cycles at util. 100%	44
$LiMn_2O_4$ // Zn foil	1 m $Zn(TFSI)_2$ + 20 m LiTFSI	1.80	119	101.2 (475)	–	–	83.8 500 cycles at util. 100%	45
$Na_3V_2(PO_4)_2F_3$@C// Zn @C	8 M $NaClO_4$ + 0.4 M $Zn(OTf)_2$	1.68	96.3	49.1 (7181)	1.060	0.540 (79.0)	100 1000 cycles at util. 78%	46
Aqueous Li-, Na-, K-ion batteries								
$LiCoO_2$/Mo_6S_8	21 m LiTFSI-0.1 wt% TMSB	2.0	120	80.0 (150)	2.160	1.440 (2.7)	92.0 100 cycles at util. 100%	47
$LiCoO_2$ array //$LiTi_2(PO_4)_3$	Sat. Li_2SO_4	1.5	93.1	69.4 (4023)	0.782	0.583 (33.8)	86.1 2000 cycles at util. 100%	48
$Na_4Fe_3(PO_4)_2(P_2O_7)$ // $NaTi_2(PO_4)_3$	17 m $NaClO_4$	1.0	36.0	20.4 (276)	–	–	75.0 200 cycles at util. 100%	49
KFeMnHCF-3565 // PTCDI	22 M KCF_3SO_3	1.2	80.0	67.0 (1612)	2.080	1.742 (41.9)	73.0 2000 cycles at util. 100%	50
Others								
β-$Ni(OH)_2$ // MH	6 M KOH	1.25	151.8	73.5 (2111)	2.581	1.250 (35.9)	82.0 1500 cycles at util. 75%	51
$Ni(OH)_2$/MWNT // FeO_x/graphene	1 M KOH	1.10	141.0	105.0 (36000)	0.254	0.189 (64.8)	80.0 800 cycles at util. 83%	52
$NiCo_2O_4$//Bi	1 M KOH	0.50	85.8	55.4 (21200)	0.121	0.078 (30.0)	89.0 1000 cycles at util. 70%	53

[a] The energy and power densities have been normalized to the total mass from both anodic and cathodic active materials. The mass of Zn plate or Zn foil anode obtained from literature is calculated based on its theoretical capacity of 824 mAh g^{-1} with an N/P=1.

[b] The cycling stability is calculated with *m* cycles at the *n*% of capacity utilization for the battery.

Table S5. Detailed parameters of various assembled 3.5 Ah Ni-Zn soft-packed batteries.

Sample N/P ratio	$m_{Cathode}$ /g		m_{Anode} /g		m_{Others}/g				m_{Total} /g	C_{max} /mAh	W / Wh kg^{-1}
	$Ni(OH)_2$	Ni foam	Zn	Cu mesh	Separator	Electrolyte	Al package	Lugs			
NiS-coated $Ni_{0.95}Zn_{0.05}(OH)_2$//Zn battery											
1.2	14.53	2.38	5.21	–	0.51	4.6	0.68	0.24	28.20	3502	211.1
1.2	14.58	2.38	5.21	0.72	0.51	4.6	0.68	0.24	28.92	3513	206.9
1.2	14.51	2.38	5.24	1.54	0.51	4.6	0.68	0.24	29.70	3523	201.7
1.6	14.63	2.38	6.80	1.54	0.51	4.9	0.68	0.24	31.68	3557	192.0
1.6	14.55	2.38	6.81	1.54	0.51	6.3	0.68	0.24	33.01	3537	183.2
2.0	14.48	2.38	9.16	1.54	0.51	7.7	0.68	0.24	36.69	3548	165.0

Various 3.5Ah Ni-Zn pouch batteries are obtained by controlling the N/P ratio, electrolyte content, and anode mass loadings. After systematic optimization, the N/P 2.0 battery shows excellent rate capability and cycling stability. When the N/P drops to 1.2, electrolyte content drops to 4.6 g, and the mass loading of Zn anode increase to 140 mg cm^{-2}, the energy density of the battery would be as high as 206.9 Wh kg^{-1}, but the rate capability is limited. So we choose the N/P 2.0 as optimal.

Table S6. Cost evaluation of the advanced Ni-Zn soft-packed battery.

	Cathode		Anode		Others				Total
	$Ni(OH)_2$	Ni foam	Zn	Cu mesh	Separator	Electrolyte	Al package	Lugs	
m_i /g	14.48	2.38	9.16	1.54	0.51	7.7	0.68	0.24	36.69
P_i	7.1391 $ kg^{-1}	11.2251 $ kg^{-1}	1.8486 $ kg^{-1}	4.7739 $ kg^{-1}	0.4285 $ m^{-2}	0.9427 $ kg^{-1}	4.2857 $ m^{-2}	11.2251 $ kg^{-1}	–
$P_i m_i$ /$	0.10288	0.02672	0.01693	0.00735	0.00900	0.00726	0.02571	0.00269	0.19855
E_d /Wh					6.05				
C $ kWh^{-1}					32.8173				

Table S7. Comparison between different types of batteries for grid-scale applications.

Types	Maturity	Voltage / V	Energy density / Wh kg^{-1}	Life	Energy Efficiency /%	Cost / US$ kWh^{-1}	Ref.
Ni-Zn	**Research**	**1.71**	**165.0**	**~2000** [a]	**90-98**	**17.79** [b] **32.90**	**This work**
Li-ion	Commercialized	3.8	80-200	1500-2000	90-94	41.12 [b] 300-2500 [c]	54, 55
Ni-MH	Commercialized	1.2	70-100	500-2500	65–70	76.34 [b] 200–729 [c]	54, 55
Ni-Cd	Mature	1.2	50–75	2000-2500	60–70	41.78 [b] 400–2400 [c]	54
Ni-Fe	Commercialized	1.2	20-50	2000-4000	50-70	39.3 [b] 72 [c]	56
V_2O_5-Zn	Research	0.8	50-80	1000-2000	85-90	56.2 [b]	40
Na-S	Commercialized	2.0	60-120	4000	75-90	300-500 [c]	54, 55
Advanced Pb-acid	Mature	2.0	30-40	500-1000	65-80	8.84 [b] 150-500 [c]	54, 55
V-based redox flow	Developed	1.2	10-20	>10000	65–70	233.66 [b] 1000-2000 [c]	54, 55
Zn-Br redox flow	Developed	1.6	70	>10000	60–65	11.15 [b] 340-1350 [c]	54

[a] The life was estimated based on the capacity loss of 0.025% per cycle of our 3.5 Ah pouch battery with a cutoff capacity of 50% at the rate of 1C. Note that when the Ni-Zn battery cycles in a low DOD level, the cycling life will be very long, e.g. over 80000 pulse cycles with 97.7% of energy efficiency within 60-80% SOC in our demo battery.

[b] Estimation of the cost based on the active materials in negative and positive electrode.

[c] The cost of the practical batteries based on the data from references.

References

1. A. Aishova, G. T. Park, C. S. Yoon and Y. K. Sun, *Adv. Energy Mater.*, 2019, **10**, 1903179.
2. P. Bonnick and J. R. Dahn, *J. Electrochem. Soc.*, 2012, **159**, A981-A989.
3. M. Gong, Y. Li, H. Zhang, B. Zhang, W. Zhou, J. Feng, H. Wang, Y. Liang, Z. Fan, J. Liu and H. Dai, *Energ. Environ. Sci.*, 2014, **7**, 2025-2032.
4. C. Xu, J. Liao, C. Yang, R. Wang, D. Wu, P. Zou, Z. Lin, B. Li, F. Kang and C.-P. Wong, *Nano Energy*, 2016, **30**, 900-908.
5. L. Zhou, X. Zhang, D. Zheng, W. Xu, J. Liu and X. Lu, *J. Mater. Chem. A*, 2019, **7**, 10629-10635.
6. H. Chen, Z. Shen, Z. Pan, Z. Kou, X. Liu, H. Zhang, Q. Gu, C. Guan and J. Wang, *Adv. Sci.*, 2019, **6**, 1802002.
7. R. Wang, Y. Han, Z. Wang, J. Jiang, Y. Tong and X. Lu, *Adv. Funct. Mater.*, 2018, **28**, 1802157.
8. Q. Gao, Z. Yuan, L. Dong, G. Wang and X. Yu, *Electrochim. Acta*, 2018, **270**, 417-425.
9. Y. Zeng, Z. Lai, Y. Han, H. Zhang, S. Xie and X. Lu, *Adv. Mater.*, 2018, **30**, 1802396.
10. W. Shang, W. Yu, P. Tan, B. Chen, H. Xu and M. Ni, *J. Power Sources*, 2019, **421**, 6-13.
11. H. Zhang, X. Zhang, H. Li, Y. Zhang, Y. Zeng, Y. Tong, P. Zhang and X. Lu, *Green Energy Environ.*, 2018, **3**, 56-62.
12. J. Li and C. Chen, *Mater. Res. Express*, 2018, **5**, 015502.
13. Q. Chen, J. Li, C. Liao, G. Hu, Y. Fu, O. K. Asare, S. Shi, Z. Liu, L. Zhou and L. Mai, *J. Mater. Chem. A*, 2018, **6**, 19488-19494.
14. Y. Zeng, Y. Meng, Z. Lai, X. Zhang, M. Yu, P. Fang, M. Wu, Y. Tong and X. Lu, *Adv. Mater.*, 2017, **29**, 1702698.
15. X. Wang, F. Wang, L. Wang, M. Li, Y. Wang, B. Chen, Y. Zhu, L. Fu, L. Zha, L. Zhang, Y. Wu and W. Huang, *Adv. Mater.*, 2016, **28**, 4904-4911.
16. J. Liu, C. Guan, C. Zhou, Z. Fan, Q. Ke, G. Zhang, C. Liu and J. Wang, *Adv. Mater.*, 2016, **28**, 8732-8739.
17. X. Wang, M. Li, Y. Wang, B. Chen, Y. Zhu and Y. Wu, *J. Mater. Chem. A*, 2015, **3**, 8280-8283.
18. Z. Lu, X. Wu, X. Lei, Y. Li and X. Sun, *Inorganic Chemistry Frontiers*, 2015, **2**, 184-187.
19. P. Hu, T. Wang, J. Zhao, C. Zhang, J. Ma, H. Du, X. Wang and G. Cui, *ACS Appl. Mater. Inter.*, 2015, **7**, 26396-26399.
20. Y. Jian, D. Wang, M. Huang, H.-L. Jia, J. Sun, X. Song and M. Guan, *ACS Sustain. Chem. Eng.*, 2017, **5**, 6827-6834.
21. J. Li, M. K. Aslam and C. Chen, *J. Electrochem. Soc.*, 2018, **165**, A910-A917.
22. J. Wen, Z. Feng, H. Liu, T. Chen, Y. Yang, S. Li, S. Sheng and G. Fang, *Appl. Surf. Sci.*, 2019, **485**, 462-467.
23. M. Huang, Z. Xu, C. Hou, S. Wang, Y. Zhuang, H.-l. Jia and M. Guan, *Electrochim. Acta*, 2019, **298**, 127-133.
24. H. Mei, Z. Huang, B. Xu, Z. Xiao, Y. Mei, H. Zhang, S. Zhang, D. Li, W. Kang and D. F. Sun, *Nano-Micro Lett.*, 2020, **12**, 61.
25. X. Ma, J. Liu, C. Liang, X. Gong and R. Che, *J. Mater. Chem. A*, 2014, **2**, 12692-12696.
26. X. Li, J. Shen, W. Sun, X. Hong, R. Wang, X. Zhao and X. Yan, *J. Mater. Chem. A*, 2015, **3**, 13244-13253.
27. M. Yu, R. Liu, J. Liu, S. Li and Y. Ma, *Small*, 2017, **13**, 1702616.
28. H. C. Chen, S. P. Jiang, B. H. Xu, C. H. Huang, Y. Z. Hu, Y. L. Qin, M. X. He and H. J. Cao, *J. Mater. Chem. A*, 2019, **7**, 6241-6249.
29. W. Wang, N. Zhang, Z. Shi, Z. Ye, Q. Gao, M. Zhi and Z. Hong, *Chem. Eng. J.*, 2018, **338**, 55-61.
30. Y. Tang, H. Shen, J. Cheng, Z. Liang, C. Qu, H. Tabassum and R. Zou, *Adv. Funct. Mater.*, 2020, **30**, 1908223.
31. L. Shen, L. Yu, H. B. Wu, X. Y. Yu, X. Zhang and X. W. Lou, *Nat. Commun.*, 2015, **6**, 6694.
32. T. Tang, S. Cui, W. Chen, H. Hou and L. Mi, *Nanoscale*, 2019, **11**, 1728-1736.
33. T. Li, G. H. Li, L. H. Li, L. Liu, Y. Xu, H. Y. Ding and T. Zhang, *ACS Appl. Mater. Inter.*, 2016, **8**, 2562-2572.
34. J. F. Parker, I. R. Pala, C. N. Chervin, J. W. Long and D. R. Rolison, *J. Electrochem. Soc.*, 2016, **163**,

A351-A355.
35. C. Xu, B. Li, H. Du and F. Kang, *Angew. Chem. Int. Ed.*, 2012, **51**, 933-935.
36. H. Pan, Y. Shao, P. Yan, Y. Cheng, K. S. Han, Z. Nie, C. Wang, J. Yang, X. Li, P. Bhattacharya, K. T. Mueller and J. Liu, *Nat. Energy*, 2016, **1**, 16039.
37. N. Zhang, F. Cheng, J. Liu, L. Wang, X. Long, X. Liu, F. Li and J. Chen, *Nat. Commun.*, 2017, **8**, 405.
38. J. Huang, Z. Wang, M. Hou, X. Dong, Y. Liu, Y. Wang and Y. Xia, *Nat. Commun.*, 2018, **9**, 2906.
39. W. Li, K. L. Wang, S. J. Cheng and K. Jiang, *Adv. Energy Mater.*, 2019, **9**, 1900993.
40. D. Kundu, B. D. Adams, V. Duffort, S. H. Vajargah and L. F. Nazar, *Nat. Energy*, 2016, **1**, 16119.
41. D. Chao, C. R. Zhu, M. Song, P. Liang, X. Zhang, N. H. Tiep, H. Zhao, J. Wang, R. Wang, H. Zhang and H. J. Fan, *Adv. Mater.*, 2018, **30**, 1803181.
42. F. Wan, L. Zhang, X. Dai, X. Wang, Z. Niu and J. Chen, *Nat. Commun.*, 2018, **9**, 1656.
43. C. F. Liu, Z. Neale, J. Q. Zheng, X. X. Jia, J. J. Huang, M. Y. Yan, M. Tian, M. S. Wang, J. H. Yang and G. Z. Cao, *Energ. Environ. Sci.*, 2019, **12**, 2273-2285.
44. J. Yan, J. Wang, H. Liu, Z. Bakenov, D. Gosselink and P. Chen, *J. Power Sources*, 2012, **216**, 222-226.
45. F. Wang, O. Borodin, T. Gao, X. Fan, W. Sun, F. Han, A. Faraone, J. A. Dura, K. Xu and C. Wang, *Nat. Mater.*, 2018, **17**, 543-549.
46. W. Li, K. Wang, M. Zhou, H. Zhan, S. Cheng and K. Jiang, *ACS Appl. Mater. Inter.*, 2018, **10**, 22059-22066.
47. F. Wang, Y. X. Lin, L. M. Suo, X. L. Fan, T. Gao, C. Y. Yang, F. D. Han, Y. Qi, K. Xu and C. S. Wang, *Energ. Environ. Sci.*, 2016, **9**, 3666-3673.
48. L. Xue, Q. Zhang, X. Zhu, L. Gu, J. Yue, Q. Xia, T. Xing, T. Chen, Y. Yao and H. Xia, *Nano Energy*, 2019, **56**, 463-472.
49. M. H. Lee, S. J. Kim, D. Chang, J. Kim, S. Moon, K. Oh, K.-Y. Park, W. M. Seong, H. Park, G. Kwon, B. Lee and K. Kang, *Mater. Today*, 2019, **29**, 26-36.
50. L. Jiang, Y. Lu, C. Zhao, L. Liu, J. Zhang, Q. Zhang, X. Shen, J. Zhao, X. Yu, H. Li, X. Huang, L. Chen and Y.-S. Hu, *Nat. Energy*, 2019, **4**, 495-503.
51. Z. Ren, J. Yu, Y. Li and C. Zhi, *Adv. Energy Mater.*, 2018, **8**, 1702467.
52. H. Wang, Y. Liang, M. Gong, Y. Li, W. Chang, T. Mefford, J. Zhou, J. Wang, T. Regier, F. Wei and H. Dai, *Nat. Commun.*, 2012, **3**, 917.
53. Y. Zeng, Z. Lin, Y. Meng, Y. Wang, M. Yu, X. Lu and Y. Tong, *Adv. Mater.*, 2016, **28**, 9188-9195.
54. M. C. Argyrou, P. Christodoulides and S. A. Kalogirou, *Renew. Sust. Energ. Rev.*, 2018, **94**, 804-821.
55. O. Schmidt, A. Hawkes, A. Gambhir and I. Staffell, *Nat. Energy*, 2017, **2**.
56. T. B. Reddy, *Linden's handbook of batteries*, McGraw-hill, New York, 2011.